Available online at www.sciencedirect.com

ScienceDirect

journal homepage: www.elsevier.com/locate/nanoenergy
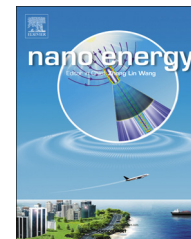
REVIEW

Piezotronic effect enhanced performance of Schottky-contacted optical, gas, chemical and biological nanosensors

Ruomeng Yu[a],[*], Simiao Niu[b], Caofeng Pan[b], Zhong Lin Wang[a],[b]

[a]School of Materials Science and Engineering, Georgia Institute of Technology, Atlanta, GA 30332-0245, USA
[b]Beijing Institute of Nanoenergy and Nanosystems, Chinese Academy of Sciences, Beijing 100083, China

Abstract
In this review, we systematically analyze the enhanced performances of Schottky-structured nanowire sensors by the piezotronic effect. Compared with traditional Ohmic-contact nanowire sensing systems, Schottky-contact provides ultra-high sensitivity and superfast response depending on the barrier height at local metal-semiconductor (M-S) interface. Utilizing the strain-induced piezoelectric polarization charges presented at the vicinity of M-S contact, piezotronic effect is applied to tune/control the charge carriers transport process through the interface by modulating the Schottky barrier height (SBH) at local contact, and thus hugely enhances the performances of Schottky-structured sensors. Our results indicate that piezotronic effect is a universal effect that provides an effective approach to improve the sensitivity, resolution, response time and other general properties of Schottky-contact nanowire sensors in different categories, including bio/chemical sensing, gas sensing, humidity sensing, temperature sensing and others.
© 2014 Elsevier Ltd. All rights reserved.

Contents

*Corresponding author.
 E-mail address: zhong.wang@mse.gatech.edu (Z.L. Wang).

Semiconducting nanowire based field effect transistors (FETs) are one of the most promising candidates for various sensing systems due to their large surface to volume ratio as well as the flexibility and convenience of functioning surface decoration [1-3]. However, most conventional semiconducting micro/nanowire-based sensors take advantage of Ohmic contact in order to maximize the surface effect. By changing resistances of the device to realize sensing performances, Ohmic structured sensors require small size micro/nanowires (both in diameter and length) in order to reduce the contact resistance as well as improve the sensitivity, which makes them extremely difficult to be manipulated or fabricated [4], because the sensitivity is dictated by the surface-to-volume ration. Later on, much more easily fabricated micro/nanowire sensors utilizing Schottky-contact structure have been demonstrated to exhibit hugely enhanced sensitivity for detecting light, gases, and biomedical species by different groups [5-12]. Unlike Ohmic-contact sensors, whose sensing performances highly depend on the changes of resistances, super-sensitive Schottky-contact sensors are achieved by tuning the Schottky barrier height (SBH) at local metal-semiconductor (M-S) interface, which dominates the carrier transport process through the whole device [13-15]. In such a case, although a large size nanowire is used the contact with the electrode is rather small, which governs the transport of the device. Therefore, by introducing piezotronic effect, which can effectively tune/control the charge carriers transport process by modulating the SBH at local contact through strain-induced piezoelectric polarization charges presenting at the vicinity of M-S interface, the performances of Schottky-contact sensors are ultimately enhanced/optimized. In this review, we introduce the basics of piezotronic effect at first, then the enhancement/optimization by piezotronic effect is systematically demonstrated by presenting a few examples of Schottky-contact micro/nanowire sensors for bio/chemical sensing, gas sensing, humidity sensing and temperature sensing.

Basics of piezotronics

Piezoelectric polarization and piezopotential

The fundamental principle of piezotronics was introduced by Wang in 2007 [16]. Piezotronics is about the devices fabricated using the piezoelectric potential as a "gate" voltage to tube/control charge carrier transport at a contact or junction. For wurtzite materials, such as ZnO, GaN, CdS and ZnS, there simultaneously exist piezoelectric and semiconductor properties. Because of their non-central symmetric crystal structure, the piezoelectric effect is produced once the material is strained. For example, ZnO has a hexagonal structure with a large anisotropic property in c-axis direction. Simply, the Zn^{2+} cations and O^{2-} anions are tetrahedrally coordinated and the centers of the positive ions and negatives ions overlap with each other. If a stress is applied at an apex of the tetrahedron, a dipole moment is generated because the center of the cations and the center of anions are relatively displaced. As shown in Figure 1b, a constructive adds up of the dipole moments created by all of the units in the crystal results in a macroscopic potential drop along the straining direction in
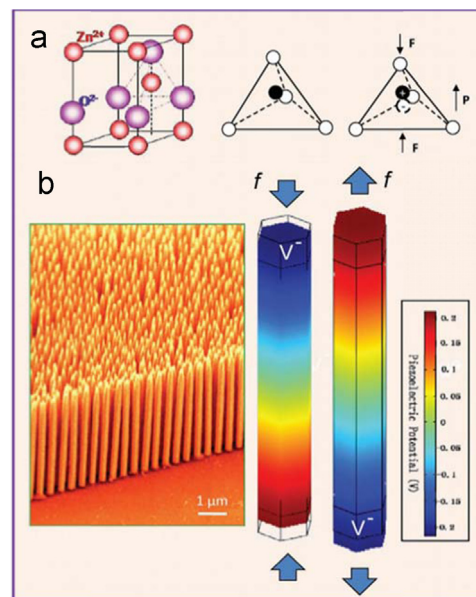
Figure 1 Piezopotential in wurtzite crystal. (a) Atomic model of the wurtzite structured ZnO. (b) Aligned ZnO nanowire arrays by solution based approach. Numerical calculated distribution of piezoelectric potential along a ZnO NW under axial strain. The growth direction of the NW is c-axis. The dimensions of the NW are $L=600$ nm and $a=25$ nm; the external force is $f_y=80$ nN. Reproduced with permission from John Wiley and Sons [65].

the crystal. This is the piezoelectric potential (piezopotential) [17].

Fundamentals of piezotronics: effect of piezopotential on metal-semiconductor contact

For a metal and n-type semiconductor contact in which the work function of the metal is larger than the electron affinity of the semiconductor, a Schottky barrier (SB) is created at the interface (Φ_{SB}). This Schottky barrier will have a rectifying effect and can only allow current to pass through if the applied external voltage is larger than a threshold value and its polarity is with the metal side positive (for n-type semiconductor). Once a strain is created in a semiconductor that also has piezoelectric property, a negative piezopotential at the semiconductor side effectively increases the local SB height to $e\Phi'$ (Figure 2b), while a positive piezopotential reduces the barrier height [17]. This piezopotential is utilized to effectively tune the local Schottky contact characteristics through the change of the Schottky barrier height and then tune/gate the charge transport properties at the metal-semiconductor (M-S) contact through external strain. This is the core working principle of piezotronics.

The performance of a Schottky contacted sensor depends on the height of the local barrier. If the barrier height is too low, it is effectively an Ohmic contact so that an adsorption of molecules at the contact will not affect the local conductance very much, resulting in low sensitivity. Alternatively, if the barrier height is too high, there is little current that can pass through the interface so that the signal is small compared with the noise. There exists an optimum height at which the sensitivity is maximized. But an as-fabricated device usually has a barrier height that is not optimum. Therefore, we can use piezotronic effect to tune the local barrier height in order to maximize the performance of the sensor. This is the main idea of our approach.

Schottky-contacted sensors

Working principle of Schottky-contacted sensors

Ever since the boost age of nanotechnology in the later of 20th century, one-dimensional semiconducting nanostructures have been extensively investigated as the basic building blocks for various sensing systems [18-28] due to their large surface to volume ratio as well as the flexibility and convenience of surface functionalization [1,29,30]. Ohmic contacts formed between metal electrodes and semiconducting nanostructures were in dominance during the early ages to maximize the output signals and gain adequate sensing performances. The sensitivity and responses of Ohmic-contacted sensors are determined by the changes of nanostructure conductance through the adsorption of analyte molecules by modification of surface charge and states [1,20] or electrostatic gating effect [23,31]. Therefore, extremely small and sophisticated nanostructures are desired to reduce the possible contact resistance for better performances, which make the fabrication process of such sensors fairly difficult and high-cost [32].

To overcome these obstacles and produce higher sensitivity, better performances sensors in much cheaper and easier manners, Schottky-contacted sensors have drawn tremendous research interests due to their outstanding sensing behavior and low-cost fabrication process. A typical Schottky-contacted sensor is built upon the well-known metal-semiconductor-metal
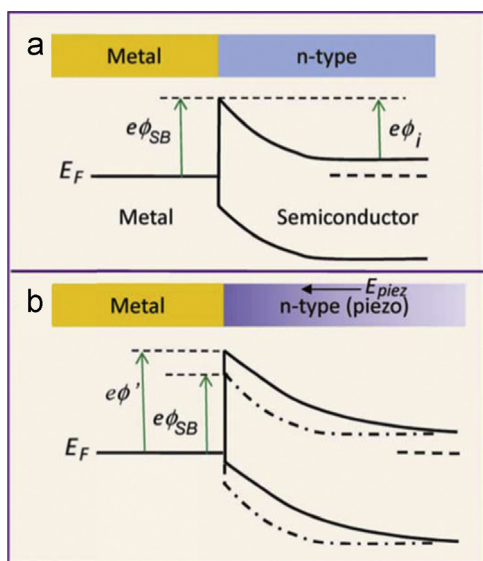
Figure 2 Energy band diagram to illustrate the effects of piezoelectricity on a Schottky contacted metal-semiconductor interface. (a) Band diagram of a Schottky contacted metal-semiconductor (n-type) interface. (b) Band diagram of the Schottky contact after applying a strain in the semiconductor. The piezopotential created in the semiconductor has a polarity with the end in contacting with the metal being low.
Reproduced with permission from John Wiley and Sons [17].
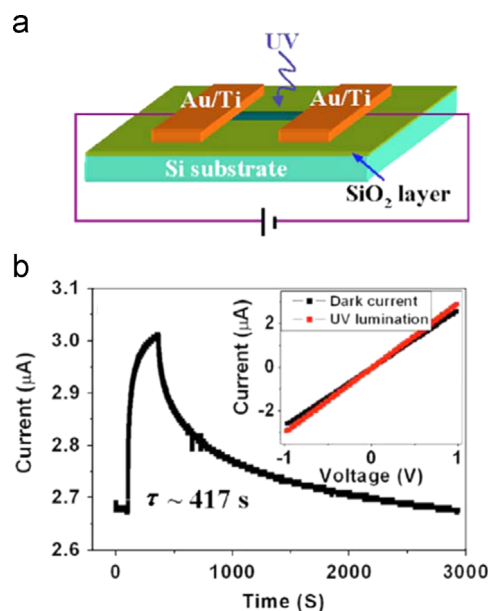
Figure 3 (a) Schematic of a ZnO NW UV sensor structure with Ohmic contacts. (b) Photon response of an Ohmic-contacted ZnO NW UV sensor at a bias of 1 V, when illuminated by 30 μW/cm^2 UV source (365 nm). The inset shows the corresponding I-V characteristics in dark and under UV illumination.
Reproduced with permission from AIP [66].

(M-S-M) structure, with Schottky contacts formed at local M-S interface. Theoretically, the charge carriers transport process through the whole device is mainly determined by the barrier height at local Schottky contact [33], therefore, these sensors are expected to perform in a more effective and sensitive manner because the adsorption of analyzed species ultimately change the Schottky barrier height (SBH) at local M-S interface rather than the conductance of nanostructure in this scenario. Compared with Ohmic-contacted sensors, same amount of analyte can definitely lead to more sensitive responses of output signals in Schottky-contacted sensors by altering the SBH instead of the bulk conductance. Therefore, Schottky-contacted sensors provide a promising strategy for designing and fabricating highly sensitive sensing systems in cheap and easy manners, based upon a fundamentally new mechanism.

Superiority of Schottky-contacted sensors

To investigate the superiority of Schottky-contacted against Ohmic-contacted sensors, our group has conducted a series of work to directly compare both types of sensors, and we concluded that Schottky-contacted sensors display gigantic enhancements in recovery time [34], response signals [11] as well as detection sensitivity [12].

Schottky-contacted UV sensor [34]

The ZnO nanowires (NWs) used for the device fabrication were synthesized by thermal evaporation method as described elsewhere [35]. UV response of our devices was characterized by a portable UV lamp (Spectroline, Model ENF-280C, 365 nm). The photon-response spectrum measurement was carried out in a PTI QuantaMaster Luminescence (QM 3PH) system. All of the measurements were carried out at room temperature in ambient condition.

To present a direct comparison of response time between Schottky and Ohmic-contacted UV sensors, we first studied the performance of an Ohmic-contact ZnO NW UV sensor. To form an Ohmic contact, Ti/Au electrodes were deposit on a single ZnO NW through shadow mask technology as schematically shown in Figure 3a. The high linear I-V characteristic (black curve in the inset of Figure 3b) of the device in dark indicated the Ohmic-contacted structure as expected. By illuminating the device using a 365 nm UV source at a power density of 30 μW/cm², the photon conductance was improved for only ∼ 15%. After about 260 s continuous illumination, the current was still unsaturated. More importantly, the reset time of the sensor was around 417 s, and the current could not recover to its initial state even after more than 2500 s (Figure 3b). Although the sensitivity of Ohmic-contacted ZnO NW UV sensor can be improved by using small size NWs, the reset time is still in the order of few hundred
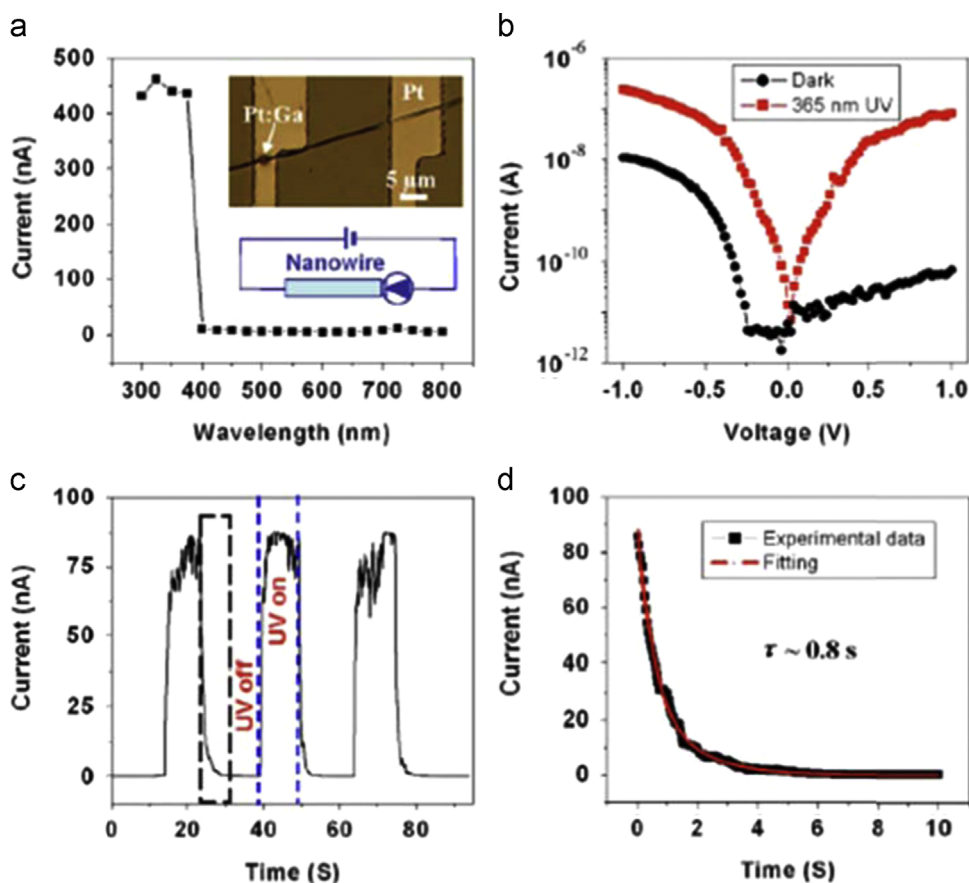
Figure 4 (a) Photon-response spectrum of the ZnO NW UV sensor as a function of wavelength of incident light. Upper inset is an optical image of Schottky-contacted UV sensor. Lower inset shows the schematic structure of the device. (b) I-V characteristics of a sensor both in the dark (black cycle) and under 365 nm UV illumination (red rectangle). (c) Time dependence of the photocurrent growth and decay under periodic illumination of the 365 nm UV light on the device. The bias on the device is 1 V. (d) Experimental curve (black) and fitted curve (red) of the photocurrent decay process Reproduced with permission from AIP [66].

seconds or even longer [36]. Such a performance is not adequate for sensor application especially used for UV detection purpose at a high frequency, thus we developed Schottky-contacted UV sensors, which are expected to have much faster response and higher sensitivity [37].

The Schottky-contacted UV sensor was fabricated by forming a Schottky barrier (SB) at local ZnO–Pt interface. A typical optical image and the schematic structure of a Schottky-contacted ZnO NW UV sensor are shown in upper and lower inset of Figure 4a. The photon-response spectrum of the device (Figure 4a) under the modulated illumination of light with wavelength ranging from 300 to 800 nm shows a sharp onset from 380 to 400 nm, corresponding to the ZnO band gap. Above the band gap energy, the photon response is almost constant, while little photon response is found from 400 to 800 nm. The high wavelength selectivity suggests that this device is intrinsically "visible-blind". Figure 4b shows typical I-V characteristics of Schottky-contacted ZnO NW UV sensors both in the dark (black curve) and upon 30 μW/cm^2 365 nm UV light illumination (red curve). The response behavior of the device were characterized by measuring the current under fixed bias of 1 V (with SB reversely biased) as a function of time when the device was periodically exposed to the UV light as shown in Figure 4c. The current increases from 0.04 to 60 nA within 0.6 s, which is nearly a 1500-fold enhancement in response. When the UV light was turned off, the current decreased to its initial state within 6 s with a reset time of 0.8 s (Figure 4d). The decay time of the photon response follows a second-order exponential decay function, with estimated time constant of τ_{d1}=0.52 s and τ_{d2}=1.47 s, and relative weight factors of 64% and 36%, respectively. The differences in response time between two types of UV sensors can therefore be attributed to the SB at the ZnO/Pt interface.

It is well known that metal Pt (work function of 6.1 eV) and n-type ZnO (work function of 5.1 eV) can form a Schottky contact, and the adsorbed oxygen at the M-S interface can significant modify the SB. Normally, the presence of a SB at M-S interface plays a crucial role in determining the electrical transport property of the M-S-M structure. At a fixed bias voltage, the voltage drop occurs mainly at the reversely biased SB [38]. When the reverse-biased Schottky contact is illuminated by 365 nm UV, photon-generated electrons and holes in the interface region are separated by the strong local electric field, thus reduce the electron-hole recombination rates and increase the carrier lifetime, resulting in an increase in free carrier density. The photon-desorption of oxygen at the ZnO/Pt interface modifies the density of defects states and, hence, alters the SB. Both of the two processes may lower the height and narrow the width of the SB, thus electrons may transit over the lowered height of the SB or tunnel through the narrowed width of the SB. This mechanism accounts for the enhanced UV response. The more rapid photocurrent decay in the ST device is mostly dictated by the electrical transport property of the SB. Upon turning off the UV light, the photon-generated electrons and holes in the interface region decreased dramatically, and the oxygen is only required to be readsorbed close to the interface to modify the SB height. It should be noted that, as the SB can be modified by many effects (such as surface absorption, strain, etc.), the long time performance stability and reliability of the ST type device may be affected, but surface passivation may protect the device.

In this work, we successfully demonstrate an effective way for improving the response time of ZnO NW UV sensors. By fabricating Schottky-contacted instead of Ohmic-contacted devices, the UV response time has been decreased from 417 to 0.8 s.

Schottky-contacted biosensor [11]

Our biosensors were fabricated using ZnO NWs grown by a vapor-solid process. For comparison purposes, we fabricated both Ohmic-contacted and Schottky-contacted devices using the same type of NWs. For the Ohmic-contacted biosensors, a single-crystal ZnO NW was placed on a Pt electrode pattern, and then Pt–Ga was deposited on both ends of the NW to form Ohmic contacts using a focused ion beam (FIB) system. The length of the NW was sufficiently long to minimize the effect from FIB contamination. The mechanism of the Ohmic-contacted sensors is to detect molecules by measuring the variation of the conductance. A sketch and a typical Ohmic-contacted I-V curve are given in Figure 5a, with the sensing responses shown in Figure 5b. We used hemoglobin as our sensing molecules; the environmental pH value was adjusted to control the electrical properties of the molecules. When the positively or negatively charged molecules were
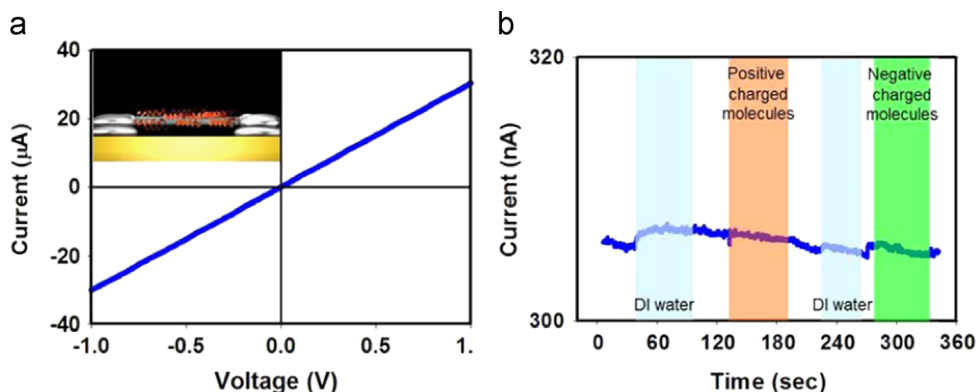
Figure 5 The Ohmic-contacted biosensor was fabricated using a single-crystal ZnO NW that shows little response to the biomolecules. (a) Pt–Ga was deposited by FIB on both ends of the NW to form Ohmic contacts (inset), as proven by its corresponding I-V curve. (b) When either positively charged molecules or negatively charged molecules are introduced, the electrical signal of the device shows little change Reproduced with permission from John Wiley and Sons [67].

introduced at a concentration of 800 mg/mL, the electrical signals of the device showed little change. This was possibly because the conductance of the ZnO NW was rather high, so that the introduction of surface-adsorbed molecules did not change the conductance to any appreciable level.

In order to enhance the sensitivity of the sensor, we deliberately introduced a Schottky contact during the device fabrication process by placing a ZnO NW on Pt electrode pattern to form a local Schottky barrier at M-S interface. A scanning electron microscopy (SEM) image of a Schottky-contacted biosensor is shown in the upper-left inset of Figure 6a. A home-built microfluidic cell was placed over the device to control the liquid environment. A typical Schottky-contacted I-V curve is shown in Figure 6a with the equivalent circuit in the lower-right inset. This device uses the adsorbed molecules to alter the Schottky barrier height (SBH) when operated under reverse bias to enhance the sensitivity. The fast reaction and distinct current variations can be seen in Figure 6b. The devices were immersed in DI water as the signal baseline for calibration purposes. The electrical response of a Schottky-contacted biosensor was characterized for a series of concentrations of charged molecules. The response of the DI water was taken as the reference line for measuring the conductance. For hemoglobin with an isoelectric point (pl) of 7.4, the molecules are negatively charged at pH 8.4 (pl<pH), and the corresponding measurement results are shown in Figure 6b. The negatively charged molecules resulted in a decrease in

conductance, as shown in Figure 6c; the detection range is from 2 fg/mL to 20 ng/mL. In contrast, when the molecules are positively charged (pH 5.6, pl>pH), an increase in conductance were observed as presented in Figure 6d, although the trend is nonlinear due to the Schottky contact. The lower detection limit is 10-20 mg/mL, and the upper detection limit is ca. 500 μg/mL. Both measurements are under a reverse bias of 2 V.

It is apparent that, as for the ZnO NW-based biosensors, the response of the Schottky-contacted construction is much larger than that of the Ohmic-contacted. Because the operation of the biosensor is largely determined by the behavior at the local Schottky barrier, which can clearly differentiate between positively and negatively charged molecules. The electrical response comes from the variation of the Schottky barrier height (SBH) and barrier width as a result of biomolecule adsorption at local M-S interface.

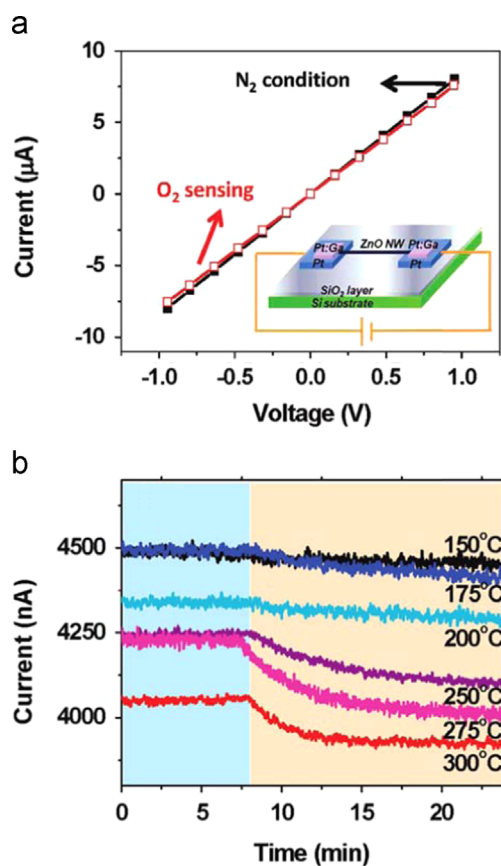### Schottky-contacted gas sensor [12]

The preparation of ZnO NWs followed the similar procedures described above. The fabrication of both Ohmic and Schottky-contacted gas sensors were carried out by forming the desired contacts between either Pt/Ga-ZnO or Pt-ZnO M-S interfaces through FIB and other standard microfabrication technologies. The gas sensing characteristics of the two types of devices, Ohmic and Schottky-contacted gas sensors, were determined via the relevant I-V curve measurements conducted at different temperatures under gas
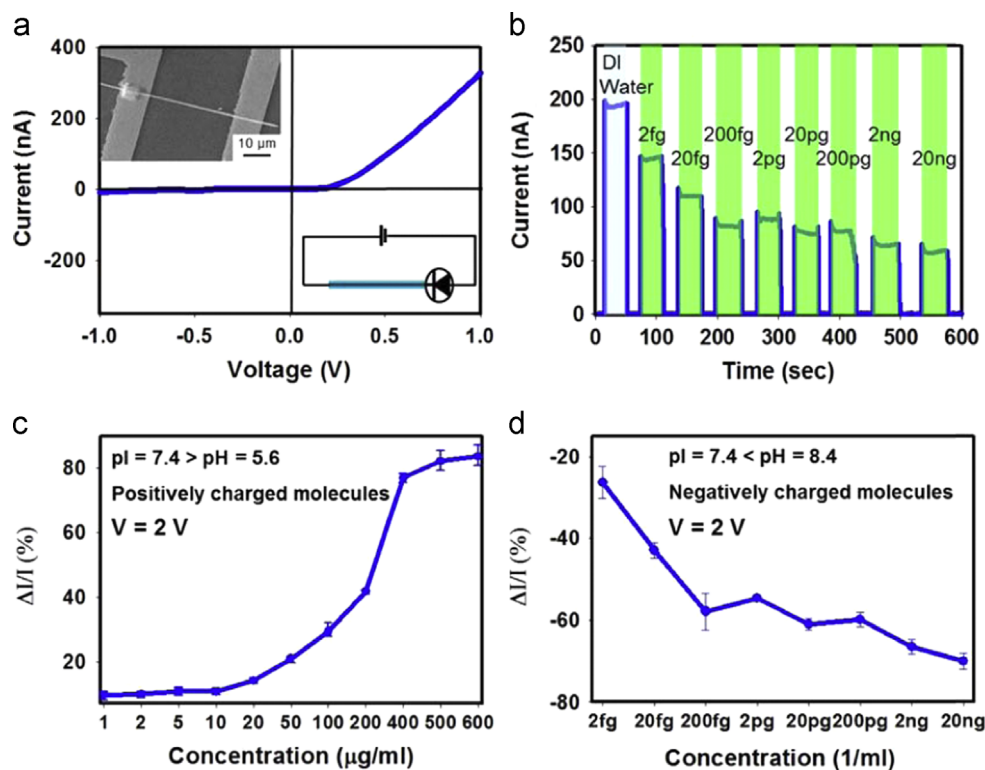
Figure 6   A Schottky-contacted biosensor uses the charged molecules to alter the SBH; the device is operated under reverse bias to enhance its sensitivity. (a) SEM image of a Schottky-contacted biosensor is shown in the upper-left inset. The I-V curve shows a typical Schottky characteristic. (b) A fast response and distinct current variations can be seen when the sensor is exposed to a series of concentrations of negatively charged molecules (pl 7.4<pH 8.4). (c) The negatively charged molecules result in a decrease in conductance. (d) When the molecules are positively charged (pl 7.4>pH 5.6), the conductance of the device increases Reproduced with permission from John Wiley and Sons [67].

atmosphere of different concentrations. The gases to be detected were O_2 and CO. The sensitivity (S) was calculated by $\Delta I / I_0$, where ΔI was the amount of current change induced after exposure of the device to the target gas atmosphere, and I_0 was the initial current.

The gas sensing characteristics of the Ohmic-contacted device toward oxygen were first investigated under a 10 wt % O_2 in N_2 atmosphere. Figure 7a shows the I-V characteristics of the Ohmic-contacted sensor recorded at 275 °C when exposed to N_2 and O_2 atmospheres. As expected, the two I-V plots appeared to be linear, showing an excellent Ohmic contact characteristic. The slopes of the two lines are, however, slightly different, with the slope of the O_2 shallower than that of the N_2. This result indicates a slightly larger resistance associated with the O_2 case, in accordance with the expected surface electron-depletion layer created by the chemisorbed oxygen species, O-, on the ZnO NW surface. Figure 7b shows I-t curves for six different system temperatures, ranging from 150 to 300 °C, and as anticipated, the current drops are rather insignificant in magnitude, corresponding to low sensitivities. Furthermore, the current responses were slow, taking several minutes to reach the next steady state. The highest sensitivity

a

b

Figure 7 (a) I-V curves measured for the Ohmic-contacted device in N_2 and O_2 atmospheres at 275 °C. Inset shows the schematic of a typical Ohmic-contacted gas sensor. (b) The response curves of the oxygen detection recorded at different temperatures, ranging from 150 to 300 °C, for the Ohmic-contacted device. The blue background denotes that the sensor was in the N_2 atmosphere and the pink background in the O_2 atmosphere Reproduced with permission from American Chemical Society [68].

of only 4.8% was obtained at a response time of 500 s for the 275 °C case. It can be inferred that the conductance decrease acquired from the adsorption of the negatively charged oxygen ions is only very minor compared to the inherent conductance of the ZnO NW.

As for the sensing performances of Schottky-contacted devices, Figure 8a shows the I-V curves measured at six different temperatures in N_2 atmosphere, evidently presenting typical Schottky contact characteristics but less pronounced with increasing system temperature. This can be attributed to the higher thermal energies of the electrons at high temperatures, retarding the rectifying function of the Schottky contact. Once the oxygen atmosphere was introduced, the conductance for both forward and reverse bias modes were decreased because of the formation of the electron-depletion layer on the ZnO NW surface (Figure 8b). With a careful comparison between Figure 8a and b, it can be concluded that the decreases in conductance achieved by the reverse bias mode were much more obvious than those produced by the forward bias mode.

The sensing response curves of Schottky-contacted gas sensors under both forward and reverse bias are presented in Figure 8c and d, respectively. It can be observed evidently from Figure 8c that the current changes of a Schottky-contacted device under forward bias were much larger in magnitude than those achieved from an Ohmic-contacted device (Figure 7b) under the same detection condition, implying much higher sensitivities for the Schottky-contacted structure. The highest sensitivity of 257% was obtained at the response time of 500 s and temperature of 275 °C, which is 54 times higher than the highest sensitivity of 4.8% achieved by Ohmic-contacted sensors under the same sensing conditions. Under reverse bias, the sensing performances of a Schottky-contacted gas sensor are shown in Figure 8d, displaying a tremendous change of current in magnitude by 2 orders from 10^{-6} to 10^{-8} ampere. A highest sensitivity of 3235% was obtained for this scenario at the response time of 500 s and temperature of 250 °C. Under the same temperature of 250 °C, the sensitivity of a Schottky-contacted device under reverse bias was 27 times higher than that of the same device under forward bias and 1085 times higher than that of an Ohmic-contacted device.

To demonstrate the capability of these sensors for CO detection, a reversely biased Schottky-contacted device was exposed to CO atmosphere of five different concentrations at 275 °C as shown in Figure 9a, where the blue region indicates O_2 conditioning and N_2 purge process, while the pink region denotes the CO sensing for duration of 60 min. It was observed that the sensitivity increased with increasing concentrations of CO, consistent with the previous reports [39-41]. The relatively slow response was mainly because of the low reaction rate between CO and O^- to form CO_2 possibly due to the trapping effect from surface/defect states. Under the same measurement conditions, an Ohmic-contacted device was also investigated as the control experiment as shown in Figure 9b. The current increased during the N_2 purge process due to the partial desorption of O^- from the NW surface. The sensitivity of the Ohmic-contacted device also increased with increasing CO concentration. From the response curves of Figure 9a and b, it is clear that the sensitivities of the Schottky-contacted gas sensor were much higher than those of the Ohmic-contacted ones. As shown in

Figure 9c and d, the sensitivity of the Schottky-contacted device was 4025 times higher than that of the Ohmic-contacted ones at a low CO concentration of 50 ppm measured; and 8776 times higher under 400 ppm, both measured at 275 °C. A highest sensitivity of 32 000% for the Schottky-contacted gas sensors was obtained at 275 °C in the CO concentration of 400 ppm.

From this work, it is concluded that the detection sensitivity of ZnO NW-based gas sensor can be significantly enhanced by employing Schottky-contact structure as an effective manner for design and fabrication of ultrasensitive NW gas sensors. By tuning the Schottky barrier height through the responsive variation of the surface chemisorbed gases and the amplification role played by the nanowire to Schottky barrier effect, an ultrahigh sensitivity of 32 000% was achieved using the Schottky-contacted device operated in reverse bias mode at 275 °C for detection of 400 ppm CO, which is 4 orders of magnitude higher than that obtained using an Ohmic-contacted device under the same conditions; and a highest sensitivity of 3235% was derived by reversely biased Schottky-contacted sensor for oxygen detection at 250 °C, which is 1085 times higher than that of an Ohmic-contacted device under the same conditions.

Piezotronic effect on Schottky-contacted sensors

From the results presented in part 2.2, we can clearly conclude that Schottky-contacted structure provides a new approach for design, fabrication and application of ultra-sensitive sensors with fast response time and outstanding response signals for various sensing systems. The Schottky Barrier Height (SBH) at local M-S interface plays a dominant role in determining the overall charge carriers transport process of these Schottky-contacted sensors. The sensitivity, response signals as well as recovery time of these sensors are all under the significant influence of the changes of SBH, which are effectively tuned/controlled through the adsorption of analyte molecules in a passive manner. However, the original barrier height of local Schottky contact is essential to the performances of these sensors. A moderate starting point of SBH leads to much better sensing performances than those unsuitable scenarios, such as relative high temperature [12] and other sever conditions. Therefore, an active method to optimize the starting point of SBH at local interface can potentially guarantee the delivery of an ultrasensitive sensor with expected performances to the maximum extent.

Piezotronic effect [17], as illustrated in part 1, is a two-way coupling effect between semiconducting and piezoelectric properties of materials with non-central symmetry, such as wurtzite and zinc blende family. Upon externally applied compressive/tensile strains, a piezoelectric potential (piezo-potential) distribution is induced inside the nanostructure along a certain crystal orientation, with piezoelectric polarization charges presented at local M-S interface in the semiconductor side. Considering the non-mobile, ionic charges nature, these strain-induced piezoelectric charges can only be partially
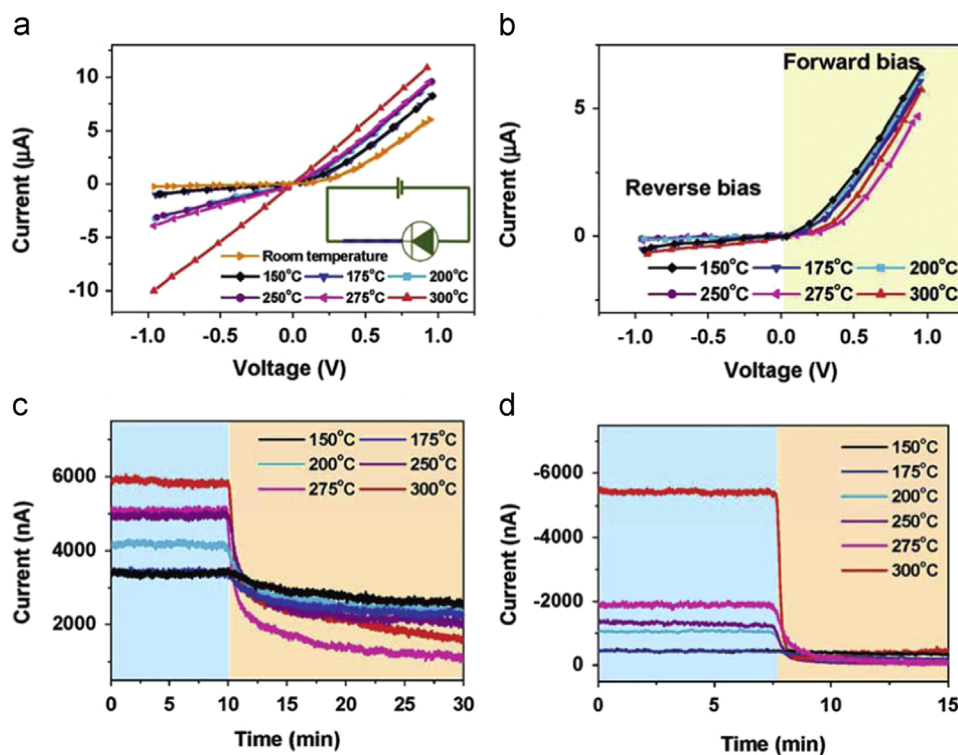

Figure 8 (a) *I–V* curves of the Schottky-contacted device measured at different temperatures in N_2 atmosphere. Inset shows the equivalent circuit of a Schottky-contacted gas sensor. (b) *I-V* curves of the Schottky-contacted device measured at different temperatures in O_2 atmosphere. (c) Response curves of the oxygen detection recorded at different temperatures, ranging from 150 to 300 °C, for the Schottky-contacted device operated under forward bias. (d) Response curves of the oxygen detection recorded at different temperatures, ranging from 150 to 300 °C, for the Schottky-contacted device operated under reverse bias Reproduced with permission from American Chemical Society [68].
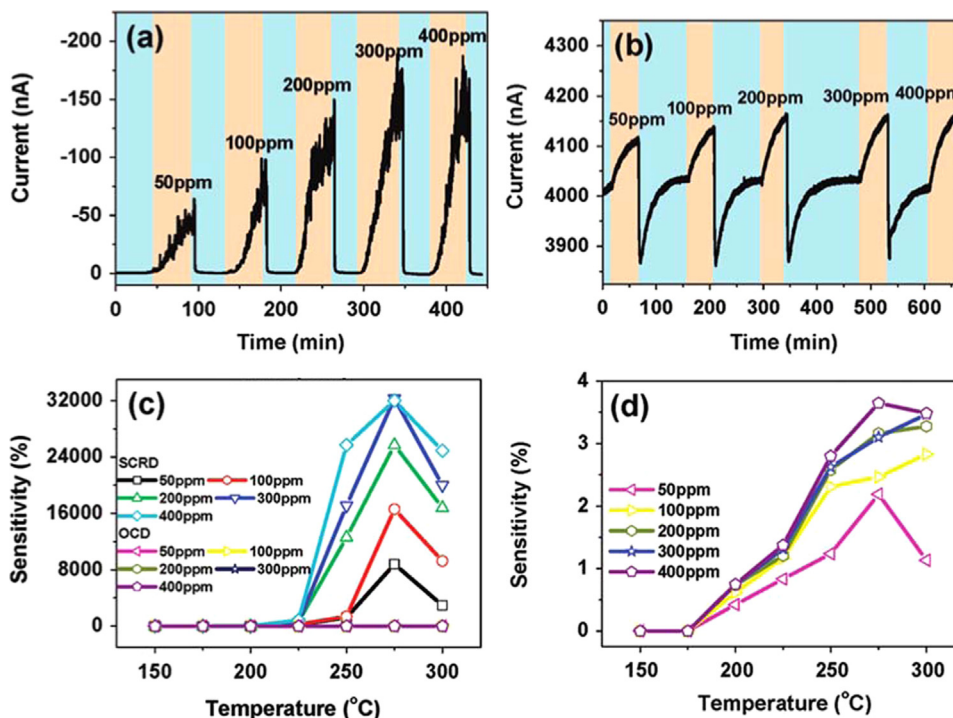
Figure 9 Response curves of the CO detection recorded at 275 °C with the device exposed to increased concentration of CO: (a) for the Schottky-contacted device under reverse bias, and (b) for the Ohmic-contacted device. (c) Sensitivity vs. system temperature for CO sensing at a response time of 1 h as a function of the CO concentration. (d) Enlarged plot of the data from panel (c) for the Ohmic-contacted device Reproduced with permission from American Chemical Society [68].
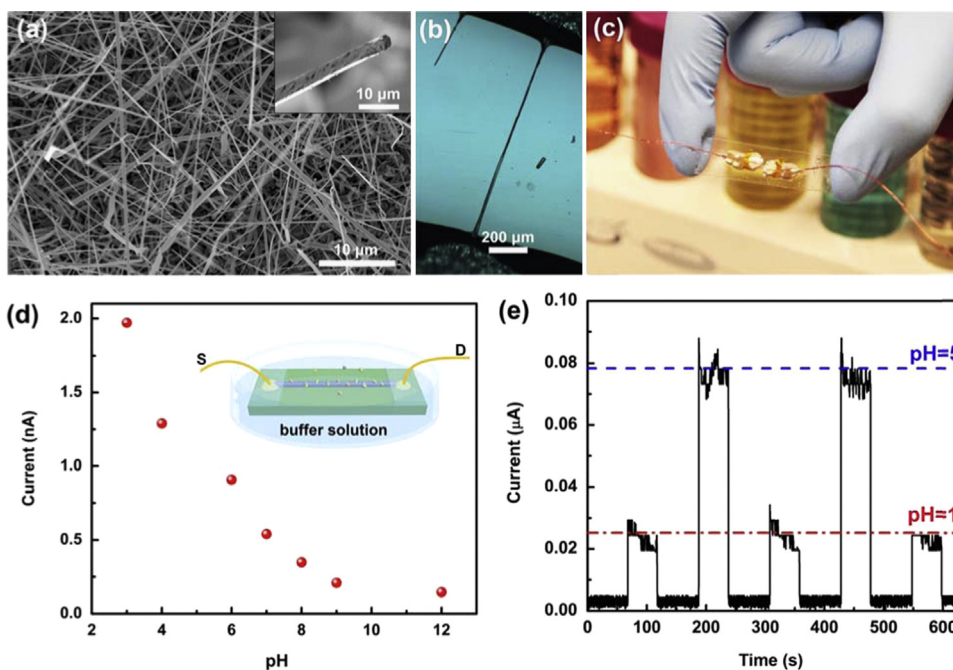
Figure 10 SEM image of the morphology of the as-synthesized ZnO NWs. The inset is a high-magnification image of an individual wire. (b, c) Optical microscopy and digital image of a ZnO NW pH sensor. (d) The response of the sensor to the pH varying from 3 to 12, no external strain was applied, just like traditional NW based sensors. (e) The repeatability of the ZnO sensor pH sensor at pH 5 and 12 Reproduced with permission from American Chemical Society [69].

screened instead of completely canceled by free charge carriers. As for Schottky-contacted sensors fabricated with piezotronics semiconductor materials, external strains can be utilized as a "strain gate" to tune/control the starting point of SBH by inducing piezoelectric polarization charges at the vicinity of local M-S interface. Therefore, we intend to

enhance/optimize the performances of Schottky-contacted nanostructure sensors by introducing piezotronic effect.

Examples of piezotronic effect enhanced Schottky-contacted sensors

A few examples are displayed below to demonstrate the piezotronics enhancement and optimization of the performances of Schottky-contacted nano-sensors from several different categories, including bio/chemical sensors (pH sensors [42], glucose sensors [43], protein sensors [44]), gas sensors [45], humidity sensors [46] and temperature sensors [47]. These results indicate that piezotronic effect is a universal effect and can be successfully applied to enhance/optimize the performances of various sensing systems based on Schottky-contact configuration.

Piezotronic effect enhanced bio/chemical sensors

Piezotronic effect enhanced pH sensors [42]
The fabrication of a ZnO NW pH sensor follows the method reported by us previously [48]. The ZnO NW was synthesized via a vapor-solid (VS) method, which gave high quality and long NWs. The morphology of the as-fabricated ZnO NWs is presented in Figure 10a, with lengths of several hundreds of micrometers and diameters varying from tens of nanometers to several micrometers. An enlarged SEM image of an individual ZnO NW is shown as an inset in Figure 10a. Then, a long ZnO NW was chosen and dispersed onto a polyethylene terephthalate (PET)/or a polystyrene (PS) substrate; both ends of the ZnO NW were fixed by silver paste, serving as electrodes as well. After that a layer of epoxy was used to fully cover the two silver electrodes, preventing them from exposing in the buffer solution during the following test. An optical microscopy image of an as-fabricated device is presented in Figure 10b, showing that the length of the ZnO NW reaches over hundreds of micrometers. A real device is given in Figure 10c.

The response of the NW sensor to the pH was tested by measuring its transportation properties in different buffer solutions. During this test, no strain was applied on the device, thus the signal level is at nA range, just like traditional NW based sensors. The results in Figure 10d demonstrate that signal of the ZnO NW sensor increased stepwise with discrete changing in pH from 12 to 3, showing a good response to the pH changing. These results are controlled by the "floating gate", and can be understood by considering the surface functionality of the ZnO NWs in different buffer solutions. At low pH, H^+ is adsorbed on the surface of the ZnO NW, and acts as a positive gate, which increases the electron carriers in the n-type ZnO NW and thus increases the conductance. At high pH, OH^- is adsorbed on the surface of the ZnO NW, which correspondingly depletes the electron carriers, and causes a decrease in conductance [1]. The response of the NW sensor to the pH changing is stable and repeatable (Figure 10e).

Figure 11 shows the stability and repeatability of the device under externally applied strain in different environments, such as in ambient and buffer solutions. Since the tensile strain could easily cause the failure of the ZnO NW, only compressive strain was applied on the device. One end of the PS substrate was fixed tightly on a manipulation holder, with the other end free to be bent. A three-dimensional (3D) mechanical stage with movement resolution of 10 μm was used to apply a strain on the free end of the PS substrate, which can be calculated according to Yang et al.'s work [49]. I-V characteristics of the devices at different strains in different solution (pH=4 and 12) were recorded in Figure 11, with the c-axis of the ZnO wire pointing from drain to source. The insets in Figure 11a, c and e are corresponding test conditions. We can find that the device has similar behaviors when it is subjected to an external strain, either in the buffer solutions or in the ambient environment. An energy band diagram of such an M-S-M structure was presented as insets in Figure 11b. It is clear that a compressive strain leads to a signal current increasing from nA to μA with a strain about −0.4% applied when the device is subjected to a bias voltage of 1.5 V, which is mainly controlled by the Schottky barrier Φ_d in such an M-S-M structure [50-53]. The Schottky barrier heights Φ_d and Φ_s at the drain and source sides in Figure 11a, c and e were quantitatively extracted through a GUI program PKUMSM developed by Peng et al. [51]. The relative changes of the Schottky barrier heights (ΔSBH) at both sides are presented at the right-hand side of Figure 11.

The signal level of the device is increased, and the sensitivity of the device is enhanced as well by the piezotronics effect, as shown in Figure 12. When a strain-free sensor was immersed in a buffer solution with pH=5, the signal level in the device was only 1.2 nA when a bias voltage of 0.5 V was applied, as the blue curve shown in the insect of Figure 12a. Thereafter, this current jumped to 1.75 μA when a compressive strain of $\varepsilon = -0.92\%$ was applied, increased by nearly 1500 times in magnitude. The responses of the ZnO NW pH sensor to the full pH changing range when the external strain was "off" (red curve) and "on" (blue curve) are presented in Figure 12b. It indicates the same phenomenon at the full pH scale that the response signal level of the device is at nA level when the ZnO NW is strain free, and the current response of the device is at μA level when the ZnO NW is compressive strained to $\varepsilon = -0.92\%$. The piezotronic effect can increase not only the signals level of the sensor, but also the sensitivity, as can be seen from the slope of the current-pH relationship in Figure 12b. Larger slope means higher sensitivity and better selectivity for the pH sensor.

The piezotronic effect increases the signal level of the device, and enhances the sensitivity of the device by tuning the effective heights of the two SBs and thus the characteristic of the NW sensor. The decrease of the Φd increases the signal current level, while the increase of the Φs decreases the signal current. As a result, two kinds of characteristic relationships between the sensor performance and the applied strain have been observed. The first one is that the signal current increases with applied strain, as shown in Figure 12c, showing the stepwise monotone increased signal current from nA to μA range at pH=4 (red curve) and 12 (blue curve). In the second case, the signal current shows a maximum in responding to the applied strain.

Piezotronic effect enhanced glucose sensors [43]
ZnO NWs used in this work were synthesized via a high temperature thermal evaporation process [33,35,54], with length of several hundreds of micrometers and diameter varying from tens of nanometers to a few micrometers. The glucose sensor was fabricated by transferring and bonding

an individual ZnO NW laterally onto a polyethylene ter-ephthalate (PET)/or a polystyrene (PS) substrate, with its *c*-axis in the plane of the substrate pointing to the source. Silver paste was used to fix the two ends of the NW, serving as the source and drain electrodes, respectively. A thin layer of epoxy was applied to isolate both end-electrodes from the environment in order to avoid potential contacting between electrodes and the glucose solution during the measurements. For the surface decoration, 0.005 ml GOx with a concentration of 10 mg/mL was added onto the NW and incubated for two hours in the fume hood to dry naturally [55], this process was repeated four times

followed by rinsing with deionized (DI) water to remove those non-firmly adsorbed GOx, then the devices were ready to perform as glucose sensors. A schematic in Figure 13a shows a GOx-decorated strain free ZnO NW glucose sensor in glucose solution. The same device under compressive strain is presented in Figure 13b. A real device is given in Figure 13c.

The response of the ZnO NW glucose sensors to different strains was investigated by applying a compressive strain step by step, up to −0.79%, with the sensors totally immersed in the pure DI water instead of glucose solution. Experiment set-up is shown in Figure 13c, one end of the
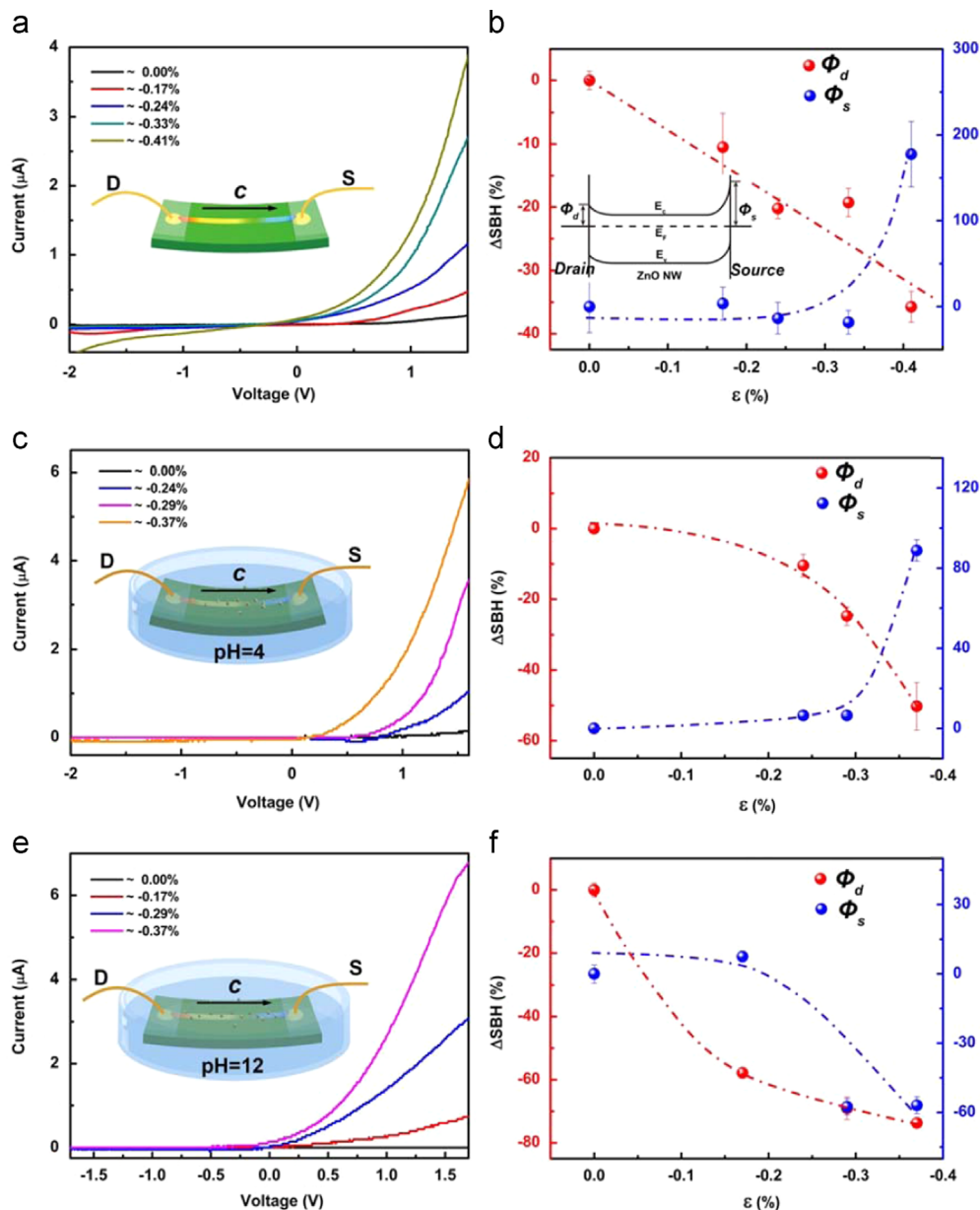
Figure 11   The stability and repeatability of the device under external applied strain in different environments, such as in ambient and buffer solutions. (a, c, e) *I-V* curves of the sensor when they are under different strains when the device is in ambient air (a), in a buffer solution pH=4 (c), and in a buffer solution pH=12 (e), with the *c*-axis of ZnO NW parallel to the longitudinal axis of the PS substrate. The right side are the corresponding relative changes of the forward and reversely biased Schottky barrier height (ΔSBH) vs. the applied strain extracted from the theoretical simulations corresponding to (a, c, e), respectively. An energy band diagram of such MSM structure is presented in (b) Reproduced with permission from American Chemical Society [69].
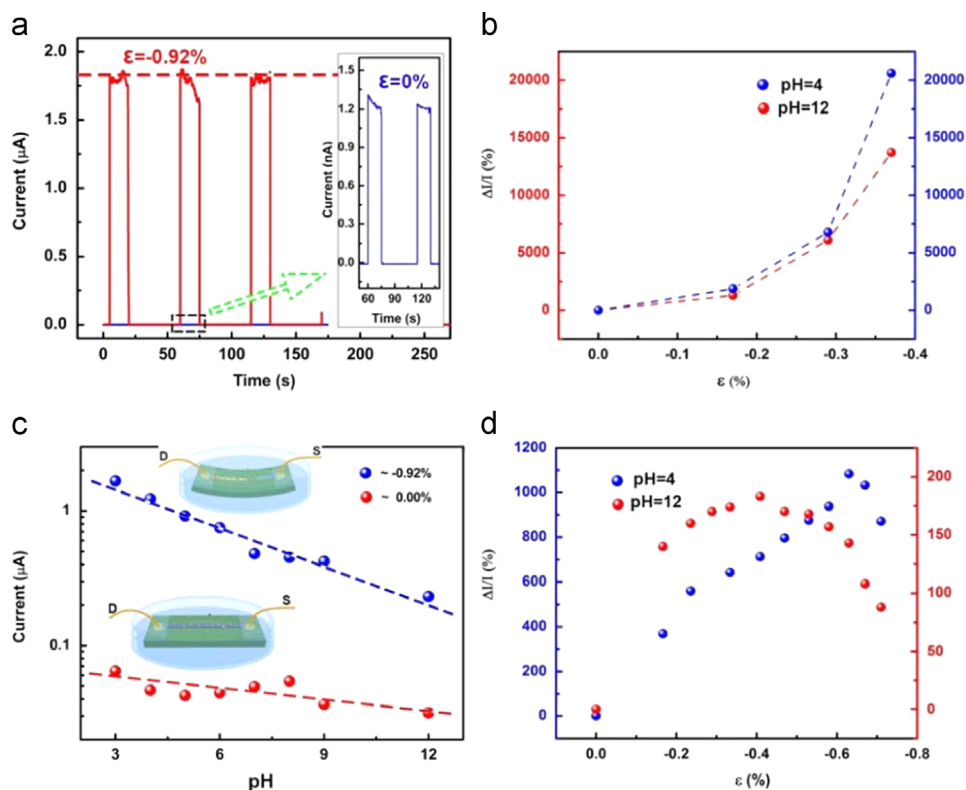
Figure 12 The signal level and the sensitivity of the sensor are increased by the piezotronics effect. (a) The output signal of a sensor in a buffer solution with pH=5 when the strain is "off" (blue) and "on" (red). The signal is increased about 1500 times when a compressive strain of $\varepsilon = -0.92\%$ was applied. (b) The response of the sensor to the pH varying from 3 to 12, when the device is strain off (red) and on (blue). (c, d) The relative change of the signal current responses to the strain applied on the device in the buffer solution with pH=4 (blue) and 12 (red), respectively, which can be divided into two categories: (c) monotone increasing, (d) the signal current showing a maximum in responding to the applied strain Reproduced with permission from American Chemical Society [69].

device was fixed tightly on a manipulation holder, while the other end was free to be bent by a three-dimensional (3D) mechanical stage with movement step resolution of 1 μm. The magnitude of compressive strains can be calculated according to Yang et al.'s work [49]. Figure 13d presents the I-V characteristics of a device when applied different compressive strains. It is obvious to see that the output signal, i.e. currents here, experienced a tremendous increase as the device was compressively bent. At a bias voltage of 1.8 V, the current increased from 0.15 μA all the way to more than 25 μA, which is about 150 times larger in magnitude, as a -0.79% compressive strain was applied.

The response of a strain free ZnO glucose sensor to different glucose concentrations is presented in Figure 13e, measured at a fixed bias of 2 V. By gradually adding glucose into the solution drop by drop, the output signal clearly increased step by step as expected. At each step, the current stayed at a distinguishable value for more than 10 seconds, which shows a good response and stability of the ZnO NW glucose sensors. Being able to response to the glucose concentrations ranging from 0.09 g L^{-1} to 1.5 g L^{-1}, the ZnO NW glucose sensor can cover the typical range of human body blood sugar level which is 0.8 g L^{-1} to 1.2 g L^{-1}, making it a qualified candidate for glucose monitoring system.

I-t and I-V characteristics of the devices at different strains and various glucose concentrations were recorded to investigate the piezotronic effect on the performances of

ZnO NW based glucose sensors. Two series of experiments were carried out by changing the strains and glucose concentrations simultaneously: the first series experiments were conducted by adding glucose solution step by step under a fixed compressive strain at each time, the I-t characteristics of a glucose sensor under compressive strain -0.33% and -0.79% are presented in Figure 14a and b, respectively. It can be seen that the overall output signals were increased by a large amount when increased the compressive strain. Moreover, it is easier to tell the current difference between two glucose concentrations as increasing the externally applied strain. This result indicates that the piezotronic effect can improve the sensing resolution of the glucose sensor, which is due to the non-linear I-V transport properties created by the Schottky barrier at the contacts of the M-S-M structure, similar to an amplification effect. By resolution here we mean the ability of the smallest concentration change that can be distinguished by the sensor and the measuring system. The second series experiments were conducted by applying compressive strains step by step in glucose solution of a certain concentration at each time, the I-V characteristics of a device in glucose solution of concentration 0 g L^{-1} and 1.67 g L^{-1} are shown in Figure 14c and d, respectively. It is obvious that the current went up by tens of times in magnitude when the glucose concentration was increased. This result again confirms the former conclusion that the
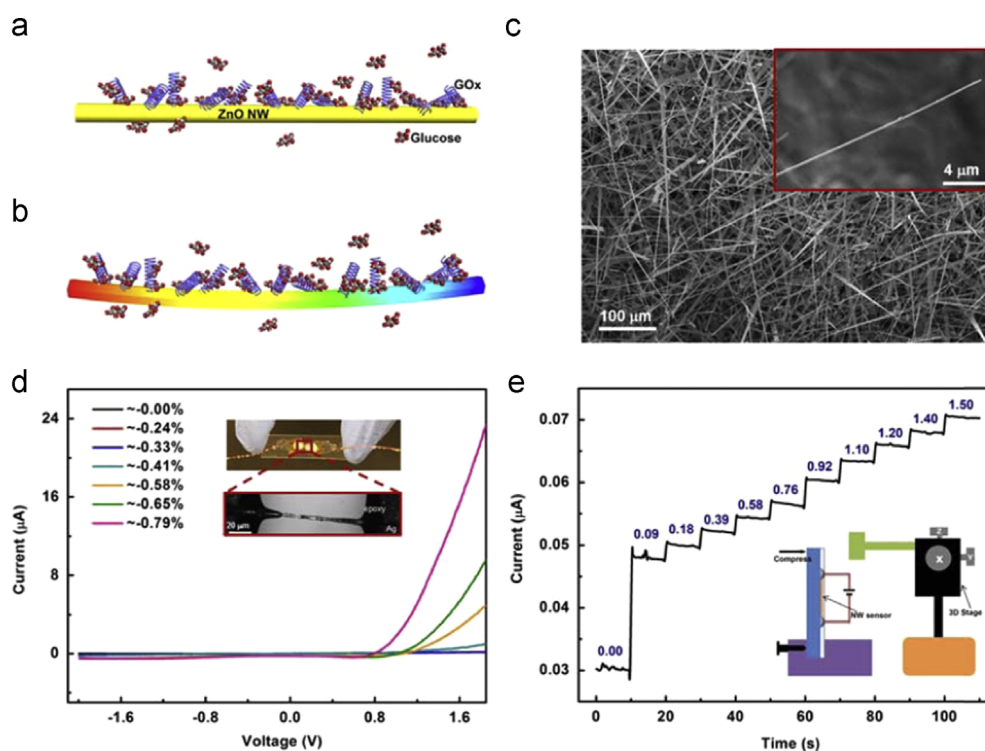
Figure 13 A schematic of ZnO NW decorated with GOx surrounded by glucose molecules under (a) no strain and (b) compressive strain. (c) SEM image of the morphology of the as-synthesized ZnO NWs. The inset presents a single ZnO NW in higher resolution. (d) *I-V* characteristics of a ZnO NW glucose sensor under different compressive strains, no glucose added. The inset shows a digital image and an optical microscopy image of the ZnO NW glucose sensor. (e) *I-t* characteristics of another ZnO NW glucose sensor in different glucose concentrations, no external strains applied. The inset presents a schematic of the experiments set-up Reproduced with permission from John Wiley and Sons [70].

higher the glucose concentration, the higher the output signals.

By systematically investigating the glucose sensors response to continuously changed compressive strains and glucose concentrations, a 3-dimensional (3D) surface graph was plotted, as presented in Figure 15a. An overall trend of how the output signal varied with changing both the compressive strains and glucose concentrations can be simultaneously derived from this 3D graph. The current clearly went up as the glucose concentration or the compressive strain increased. Four 2D graphs are shown in Figure 15b-e for more details and information, which are extracted from Figure 15a by projecting on I-Strain surface and I-Glucose concentration surface, respectively. Figure 15b and c shows the absolute and relative current response of ZnO NW glucose sensors to various glucose concentrations when the compressive strain was fixed in each curve, ranging from -0.00% to -0.79%, respectively. Figure 15d and e presents the absolute and relative current response of ZnO NW glucose sensors to different compressive strains under a certain glucose concentration in each curve, differing from $0.00\,g\,L^{-1}$ to $1.50\,g\,L^{-1}$ step by step. The results in Figure 15b show that the slope of curves became deeper and deeper when the applied strain increased, which means the sensing resolution is improved by the piezotronic effect. The same improvement can be derived more easily from Figure 15d, which indicates that the current difference between two certain glucose concentrations was significantly enlarged when applying more compressive strain. From Figure 15c it can be seen, the relative change in current by

adding glucose can be as large as 130% and mostly around 25% to 50%. In Figure 15e, this relative change in current has the largest value more than 300% and mostly around 150%, when applied more compressive strains. These results indicate that, applying strains can significantly improve the sensitivity of glucose sensors, the relative change of output signals in this case is even much larger than that in the case of adding glucose. Therefore, the performance of the glucose sensor was generally enhanced by the piezotronic effect when applying a -0.79% compressive strain on the device, and the output signal level was increased by more than 200% in magnitude; the sensing resolution and sensitivity of sensors were improved by more than 200% and 300%, respectively.

Piezotronic effect enhanced protein sensor [44]

ZnO NWs used in this experiment were synthesized via a high temperature thermal evaporation process [33,35,54], with length of several hundreds of micrometers and diameter ranging from tens of nanometers to a few micrometers. The device was fabricated by transferring and bonding an individual ZnO NW laterally onto a PET/PS substrate, with its *c*-axis in the plane of the substrate pointing to the source. Silver paste was used to fix the two ends of the NW, serving as source and drain electrodes as well, respectively. For such a Ag-ZnO NW-Ag device, it could be treated as a metal-semiconductor-metal (M-S-M) structure [33]. A thin layer of epoxy was used to fully cover both end-electrodes in order to rule out possible contacting
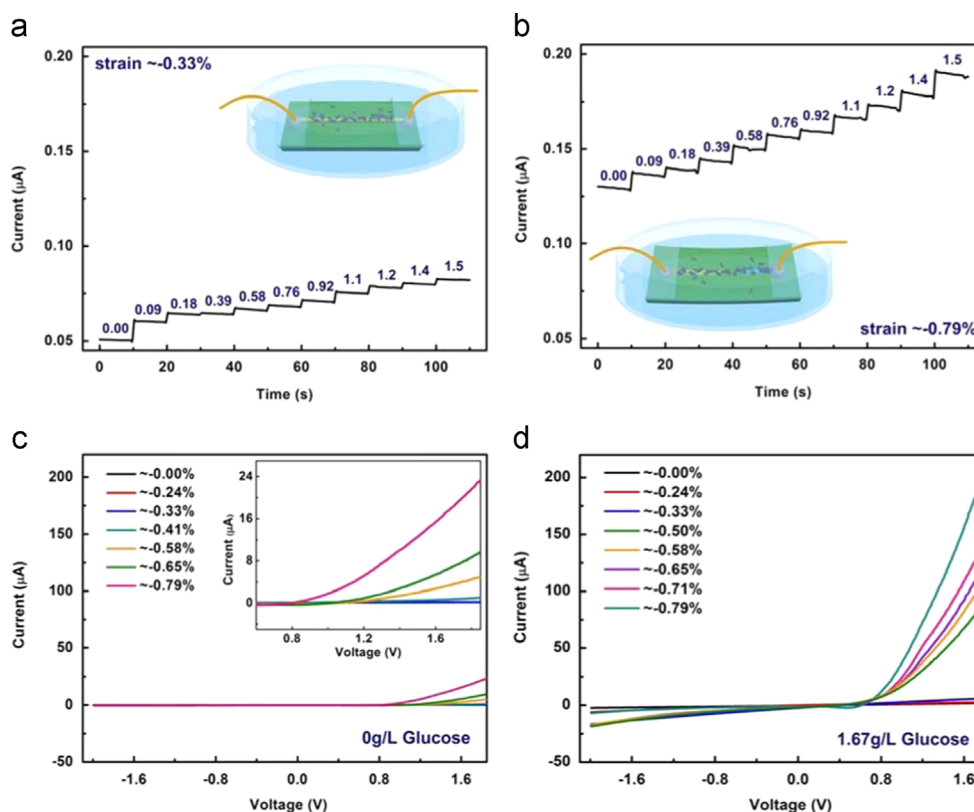
Figure 14 *I-t* characteristics of a ZnO NW glucose sensor in different glucose concentrations, numbers labeled in unit of (g L^{-1}), under (a) -0.33% compressive strain and (b) -0.79% compressive strain. The insets are schematics of adding glucose step by step to the glucose sensor under -0.33% and -0.79% compressive strain, respectively. *I-V* characteristics of the ZnO NW glucose sensor under different compressive strains, in a certain glucose concentration of (c) 0 g L^{-1} and (d) 1.67 g L^{-1}. The inset of (c) is an enlarged *I-V* curve to present more details Reproduced with permission from John Wiley and Sons [70].

between electrodes and the solution when the device is immersed into protein solution. Then gold nanoparticles-anti-Immunoglobulin G conjugates (Au NP-anti-IgG) was assembled onto the surface of ZnO NW by adding 0.01 ml of Au NP-anti-IgG colloidal solution (purchased from Tedpella, used directly without further purification) on the NW and incubated for one hour in the fume hood. Before carrying out protein Immunoglobulin G (IgG) test, the devices were modified with a blocking buffer (BB) (0.1% Tween 20 (purchased from Tedpella), 0.1% fish gelatin (purchased from Tedpella), and 1% BSA (purchased from Sigma-Aldrich)). It was reported that BB could efficiently block the nonspecific binding of IgGs to the devices [56]. Thus, treating the device with BB can effectively diminish the undesirable response from the nonspecific binding to the device and is necessary for the specific function of the sensor. Devices with BB were dried for two hours at room temperature and then washed with PBS buffer. After that, 0.005 mL of IgG (Sigma-Aldrich) sample with a given concentration was pipetted onto the device for protein binding for one hour, followed by washing and drying. A schematic in Figure 16a shows the principle of a strain free and Au NP-anti-IgG decorated ZnO NW protein sensor, with target protein IgG bonded. The same device applied by external compressive strains is presented in Figure 16b.

The response of the ZnO NW protein sensor on different IgG concentrations is presented in Figure 16c, which was measured at a fixed bias of 2 V. The response signal of the device (i.e. current here) increased significantly from nA scale to several μA with the increasing of the targeting protein IgG concentrations from 0 to 1E−3 g/mL, since more target protein IgG being adsorbed onto the surface of the ZnO NW. This result indicates that the Anti-IgG decorated ZnO NW device has a good response to IgG concentrations. Further detailed examinations were carried out by measuring the current-voltage (*I-V*) curves of the sensor, with a bias voltage ranging from −2 to 2 V. *I-V* curves of a ZnO NW device under different IgG concentrations are presented in Figure 16d, which indicates that the output signals of the device are much stronger at higher IgG concentrations.

Piezotronics effect on the performance of these ZnO NW sensors was examined under compressive strains, which can be calculated according to Yang et al.'s work [49]. Figure 17 shows four sets of *I-V* curves corresponding to different IgG concentrations with protein sensors under compressive strains. Take Figure 15a as an example to illustrate how piezotronic effect tuned the performance of ZnO NW protein sensors. The current increase obviously, and the shape of *I-V* curves changes from an "Ohmic type" to the "Schottky type" when the externally applied strain increased from 0%, −0.41%, −0.58%, −0.67%, −0.75% to −0.82% [49]. Similar trends are observed for all the other three sets of *I-V* curves. It is necessary to notice that, the variation of the *I-V* curves of ZnO biosensors was attributed to a combination of bulk resistance change (piezoresistance effect) and the piezotronic effect, as reported in previous
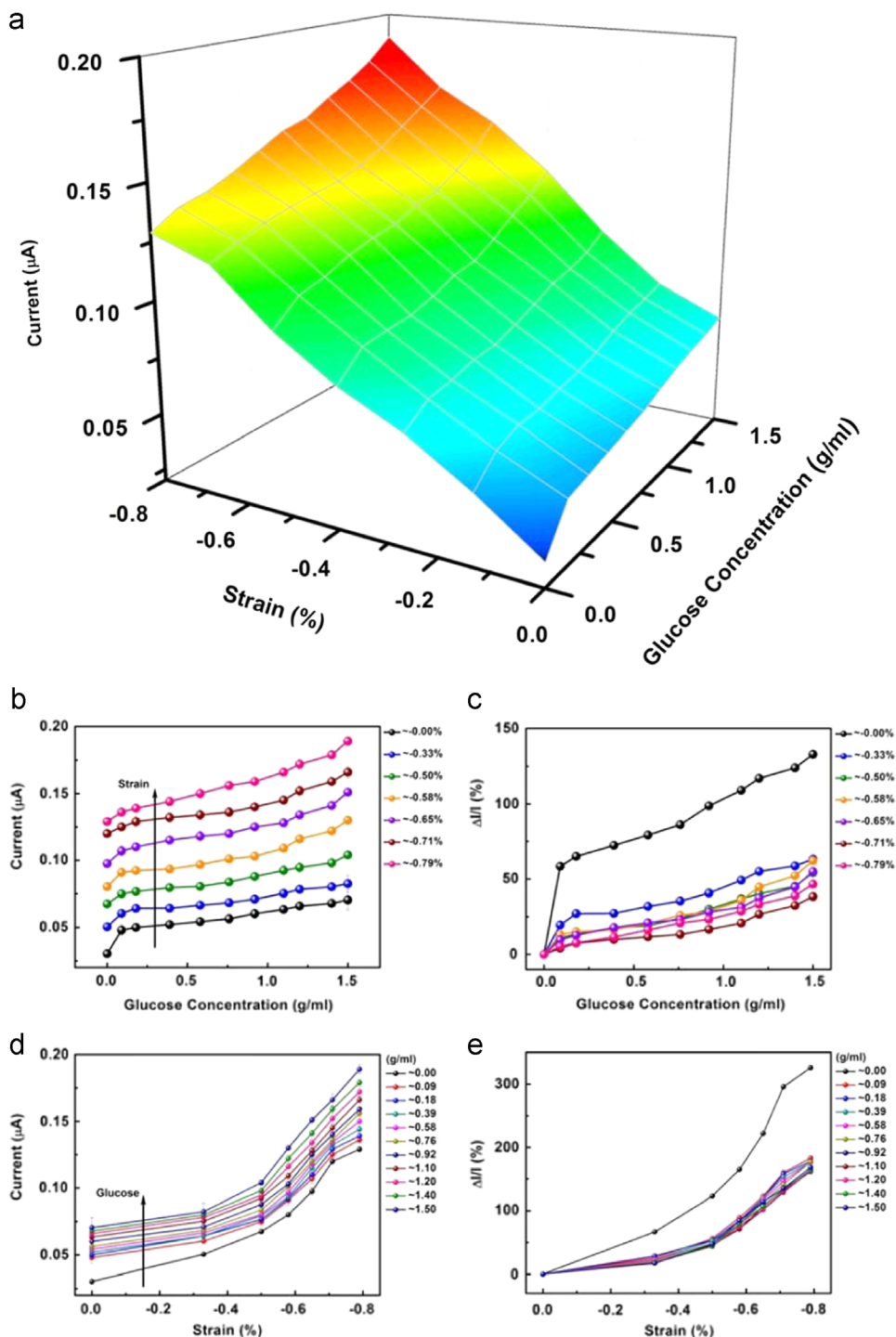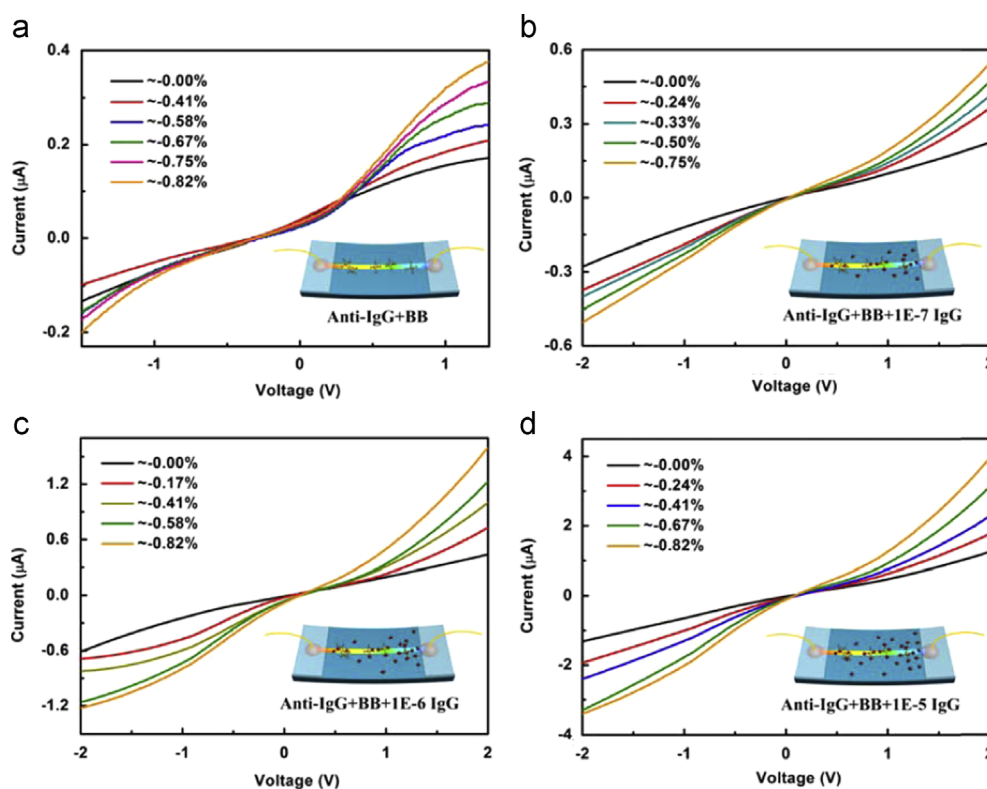
Figure 15 Piezotronic effect on the performances of ZnO NW glucose sensors. (a) 3D surface graph indicating the current response of the ZnO NW glucose sensor under different strains and glucose concentrations. (b, c) Absolute and relative current response of the ZnO NW glucose sensor in different glucose concentrations, with compressive strain ranging from 0% to -0.79%, respectively. (d, e) Absolute and relative current response of the ZnO NW glucose sensor under different compressive strains, with glucose concentration ranging from 0 to $1.50\,\mathrm{g\,L^{-1}}$, respectively. Data of (b-e) were extracted from (a) Reproduced with permission from John Wiley and Sons [70].

work [57]. In our case, the piezoresistance effect effectively lowered down the barrier heights at both ends, hence increased the output currents at both $+2\,\mathrm{V}$ and $-2\,\mathrm{V}$; on the other hand, piezotronic effect increased the output current at $+2\,\mathrm{V}$, while decreased that at $-2\,\mathrm{V}$. I-V curves shown in Figure 17 were derived under the influence of both piezotronic
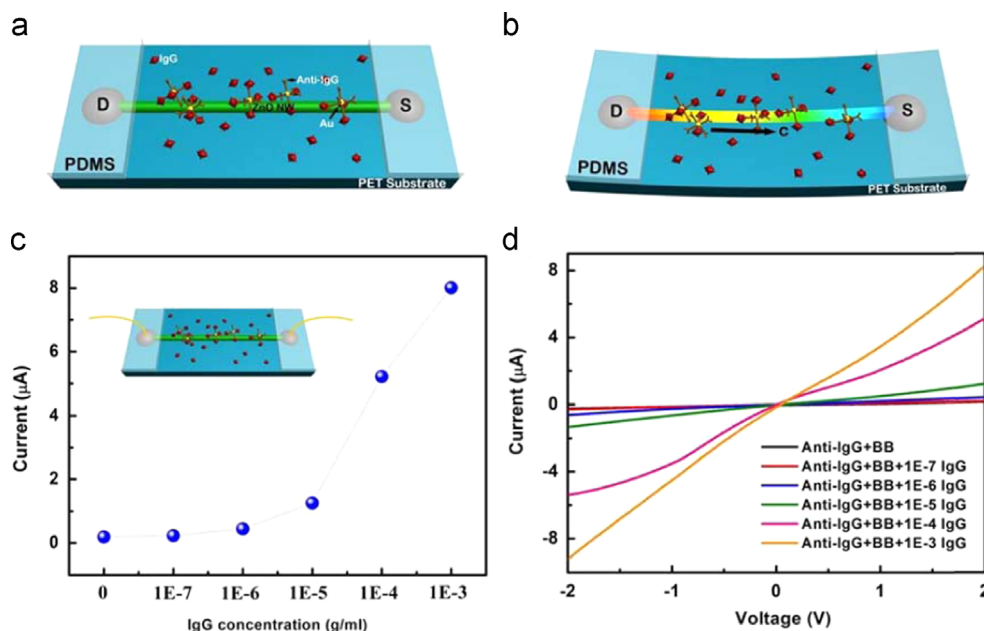
Figure 16 Schematic and target protein IgG response of a ZnO NW sensor. (a) Gold nanoparticle-anti-IgG surface functionalized ZnO NW protein sensor bonding with target protein IgG. (b) ZnO NW protein sensor under compressive strain. (c) Target protein IgG response of ZnO NW devices at a fixed voltage of 2 V, with the IgG concentration varying from 0 to $1E-3$ g/mL, no external strain was applied. Inset is a schematic of the corresponding ZnO NW device. (d) *I-V* curves of ZnO NW devices at different IgG concentrations, no external strain was applied Reproduced with permission from Royal Society of Chemistry [71].

Figure 17 *I-V* curves of the ZnO NW protein sensor under different degrees of compressive strain, when the device was decorated with (a) anti-IgG and BB, (b) anti-IgG and BB bonding with $1E-7$ g/mL target protein IgG, (c) anti-IgG and BB bonding with $1E-6$ g/mL target protein IgG, (d) anti-IgG and BB bonding with $1E-5$ g/mL target protein IgG. Insets are the schematics of corresponding ZnO NW devices Reproduced with permission from Royal Society of Chemistry [71].
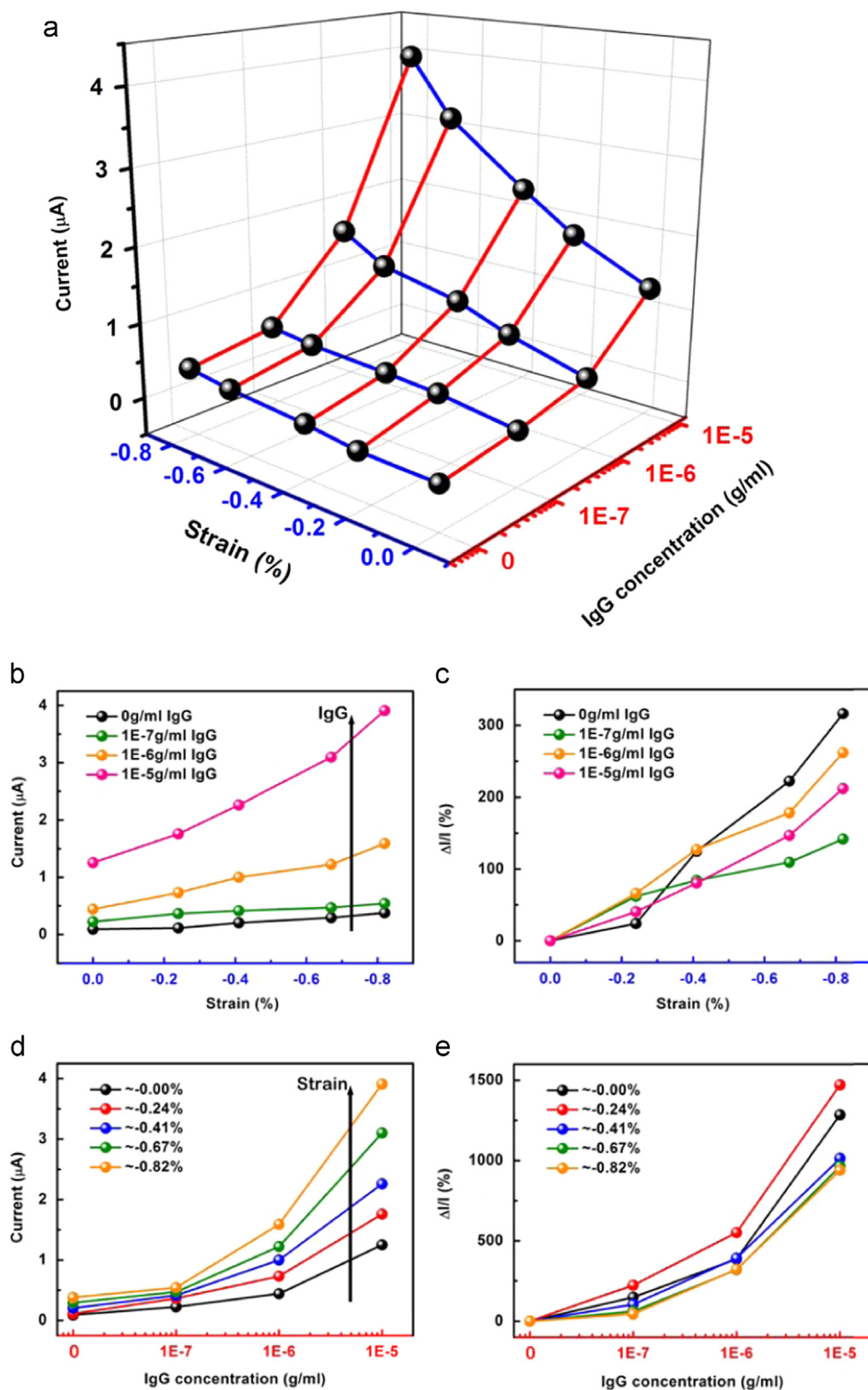
Figure 18 Piezotronic effect on the performances of ZnO NW protein sensors. (a) 3D graph depicting the current response of ZnO NW protein sensor under different strains and IgG concentrations. (b, c) Absolute and relative current response of ZnO NW protein sensor under different compressive strains, with IgG concentration ranging from 0 to 1E−5 g/mL, respectively. (d, e) Absolute and relative current response of ZnO NW protein sensor at different IgG concentrations, with compressive strain ranging from 0% to −0.82%, respectively. Data of (b–e) were extracted from (a) Reproduced with permission from Royal Society of Chemistry [71].

effect and piezoresistance effect, dominated by piezotronic effect though [50,58]. Therefore, the *I-V* curves here are not similar to those of a diode, but the relative change of currents at +2 V is larger than that at −2 V, since the barrier height was decreased by both of two effects at one end, while increased by piezotronics effect and decreased by piezoresistance effect at the other end. The change in transport characteristics indicates that the piezotronic effect in ZnO NW tunes the effective height of the Schottky barrier at local contacts, which played a very important role in tuning the performance of protein sensors. The non-linear effect introduced by piezotronic effect in current transport can significantly enhance the sensitivity of the sensor.

By systematically investigating the sensor response on the changing external strain and targeting protein concentration, the results were extracted and plotted in a 3-dimentional (3D) graph, as shown in Figure 18a. It is straightforward to see that current increases as the IgG concentrations or compressive strains increases. Four 2D graphs are shown in Figure 18b-e for more details and information, which are extracted from Figure 18a by projecting on *I-Strain* surface and *I-IgG* concentration surface, respectively.

Figure 18b and c shows the absolute and relative current response of ZnO NW protein sensor under different compressive strains when the concentration of target protein was fixed at 0, 1E−7, 1E−6 and 1E−5 (g/mL), respectively. These 2D graphs present four curves at four IgG concentrations, each was derived by measuring the output current of ZnO NW protein sensor under different compressive strains. For each curve, as increasing the strain, the difference between currents related to two adjacent IgG concentrations was enlarged. It means that the piezotronic effect largely enhanced the resolution of the protein sensors, which is the result of the non-linear *I-V* transport properties as created by the Schottky barrier at the contacts of the M-S-M structure. Figure 18d and e presents the absolute and relative current response of ZnO NW protein sensor at different IgG concentrations, with compressive strain fixed in each curve, ranging from 0 to −0.82%, respectively. It can be seen from this graph that at a fixed IgG concentration, the larger the strain

the higher the output current: at a very low IgG concentration, without applying external strains, the output current might be too small to be detected, while applying a compressive strain; the output signal could be enhanced large enough to be detected. That is to say, piezotronic effect can improve the detection limit or sensitivity of ZnO NW protein sensors.

Piezotronic effect enhanced gas sensor [45]

ZnO NWs used in this work were grown by a vapor-solid method at 1465 °C [35]. Figure 19a shows a typical scanning electron microscopy (SEM) image of the as-grown ZnO NWs. To fabricate an oxygen sensor, a long ZnO NW (100-300 μm in length and around 800 nm in diameter) was chosen and transferred onto a flexible PET substrate (1 cm × 5 cm, 220 μm in thickness), with its *c*-axis parallel to the long edge of the substrate. Both ends of the NW were then fixed with silver paste to form an M-S-M structure. A typical optical image of an as-fabricated oxygen sensor is shown in Figure 19b. A schematic of the measurement setup is sketched in Figure 19c. One end of the device was tightly fixed on a bracket inside a gas chamber. Strain was introduced by moving a positioner to bend the device at the other end. The positioner can be controlled outside of the chamber with a displacement resolution of 0.5 mm. A UV lamp (central wavelength=254 nm, power=23 W) was placed facing the quartz window outside of the chamber. Before the measurement, the device was first maintained under vacuum for 10 min. A 254 nm UV light was then applied on the device for half an hour for pre-removal of oxygen on the device [59]. Finally, the electrical measurement of this device was performed after the UV light was turned off for about 1 h.

Systematic measurements of the oxygen sensor were performed in a pure oxygen atmosphere under different oxygen pressures and different strain conditions at room temperature. Figure 20a and b shows the oxygen sensor performance under 0% strain and 0.2% tensile strain
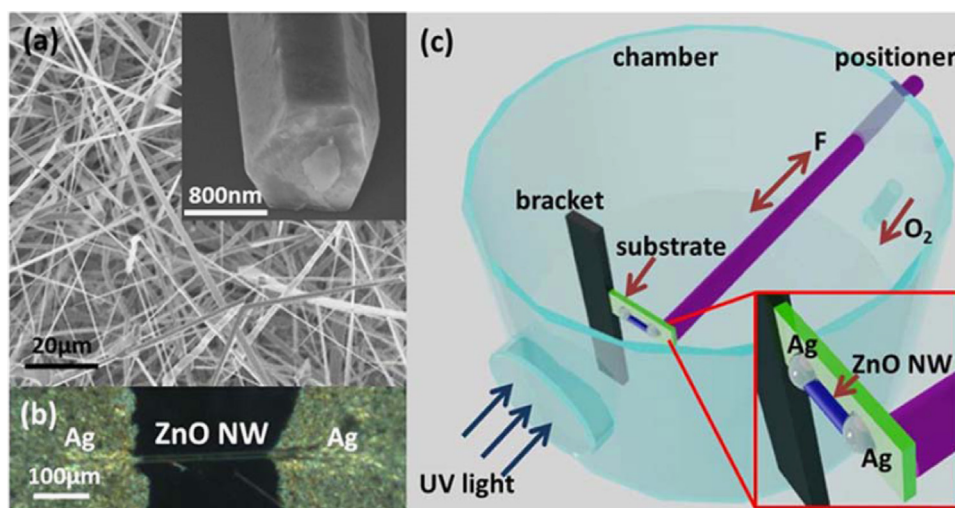

Figure 19 (a) SEM images of ZnO NWs. The inset is a high-magnification image of an individual wire. (b) Optical microscopy image of a typical ZnO NW oxygen sensor device. (c) Schematic of the measurement set-ups for studying the piezotronic effect in a ZnO NW oxygen sensor. Reproduced with permission from John Wiley and Sons [16].

conditions at different oxygen pressures. The device shows a typical non-linear nonsymmetrical *I-V* curve, which indicates that the two Schottky barriers at the two contacts have different heights. As for the M-S-M structure, these two Schottky barriers are connected back to back through the NW. Under positive or negative bias voltage, only the reversely biased Schottky barrier will dominantly control the transport properties. The current drops under both bias conditions when the oxygen pressure increases, which agrees with our former work and can be explained by the following reasons [12]. First, due to the adsorption of oxygen, the electron depletion layer is formed on the ZnO NW surface, which reduces the carrier density in the NW. In particular, the oxygen adsorption around the Schottky contact area raises the SBH and thus reduces the overall current. While under − 1 V bias condition, the current drops even more. These distinctly different responses under positive and negative bias voltage indicate that this relative current change depends on the SBH. Figure 20c and d shows the oxygen sensor performance at 16 Torr and 500 Torr oxygen pressure under different strain conditions. The obviously non-symmetric change of current under positive and negative bias voltage is due to the piezotronic effect, as reported in our previous research [33,44]. For the piezotronic effect, the SBH at the contact with positive piezocharges decreased, while the SBH at the other contact with negative piezocharges increased. While for the conventional piezoresistive effect, the change in resistance is a symmetric effect under both forward and reverse bias. These

two effects combine together and generate a non-symmetric decrease of current at both sides.

To show the oxygen sensor's performance better, a 3D graph is plotted and shown in Figure 21a and c. As previously presented, the current drops with the increase of either oxygen pressure or tensile strain. The relative current change of this oxygen sensor under both bias conditions is calculated and summarized in Figure 21b and d. Under 0 strain and − 1 V applied bias, this device can show a relative current change of − 87.3% from 16 to 500 Torr. This sensitivity is much better than the existing ZnO oxygen sensor that can work at room temperature [60-62]. The high sensitivity of our device is mainly due to two reasons. First, the Schottky barrier formed between the ZnO NW and silver can significantly enhance the sensitivity. In a Schottky diode under moderate reverse bias, the current has an exponential relationship with the SBH. Thus, utilizing a Schottky diode can greatly enhance the sensitivity. Second, the pre-removal of oxygen by UV light improves the adsorbability of oxygen on ZnO NW surfaces. The UV light can generate electron-hole pairs at the ZnO NW surface [59]. The holes can combine with O_2^- and form an oxygen molecule. Therefore, the O_2^- ions at the ZnO NW surface can be effectively removed by UV light. Once the UV light is off, the UV-treated ZnO NW surface is more favorable for adsorbing oxygen, which improves the sensitivity. This relative current change is further enhanced by applying a tensile strain. Under the positive bias, the relative current change at oxygen pressures from 16 to 700 Torr enhances
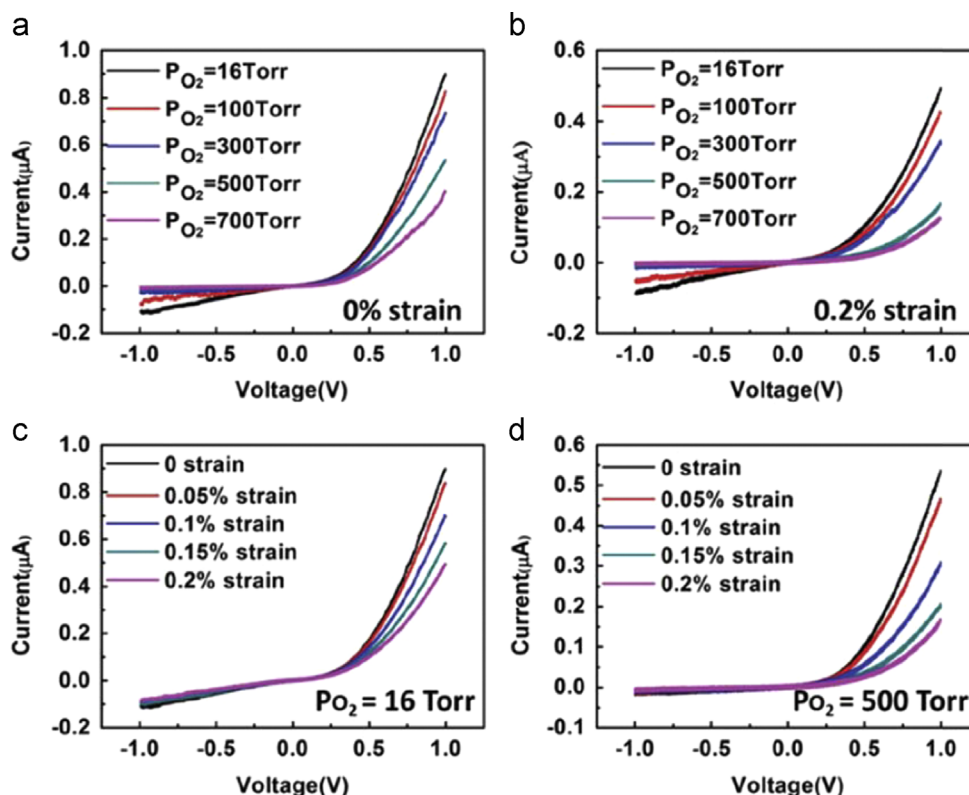
Figure 20 *I-V* curves of the oxygen sensor under different strain and oxygen pressure conditions: (a) Under 0% strain and different oxygen pressure from 16 to 700 Torr. (b) Under 0.2% tensile strain and different oxygen pressure from 16 to 700 Torr. (c) Under 16 Torr oxygen pressure and different tensile strain from 0% to 0.2%. (d) Under 500 Torr oxygen pressure and different tensile strain from 0% to 0.2% Reproduced with permission from John Wiley and Sons [16].
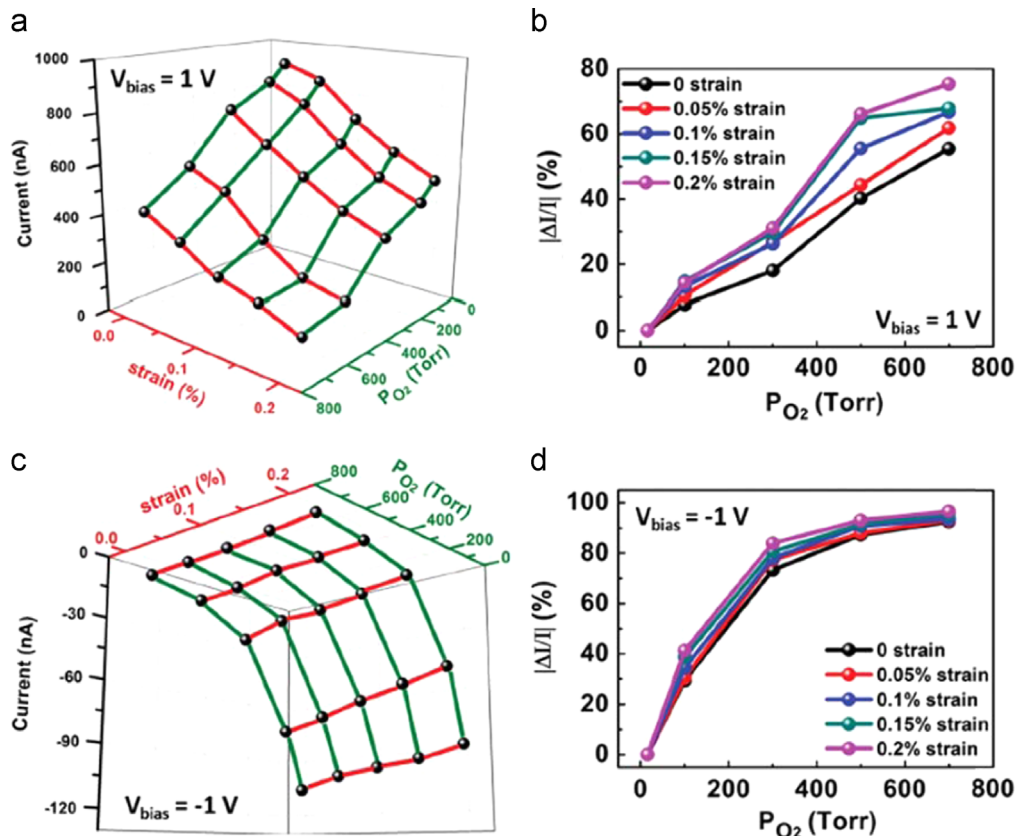
Figure 21 Piezotronic effect on the performance of an individual ZnO NW-based room temperature oxygen sensor. (a) 3D graph depicting the current response of the ZnO NW oxygen sensor under different strains and oxygen pressures at a bias voltage equal to 1 V. (b) Magnitude of relative current change with oxygen pressure under different tensile strain from 0% to 0.2% at a bias voltage of 1 V. (c, d) corresponding results of figure (a, b) at bias voltage of −1 V Reproduced with permission from John Wiley and Sons [16].

from −55.4% to −75.4%, respectively, as the applied tensile strain increases from 0% to 0.2%. Under the negative bias, the relative current change at oxygen pressures from 16 to 700 Torr increases from −87.3% to −93%, respectively, as the applied tensile strain increases from 0% to 0.2%. Therefore, by applying a tensile strain, the already very high sensitivity due to the Schottky-contact structure and pre-treatment of UV light is even further enhanced by piezotronic effect.

Piezotronic effect enhanced humidity sensor [46]

ZnO nanowires (NWs) were grown by a vapor–liquid–solid process at 960 °C, showing a hexagonal cross section with several hundred micrometers in lengths and hundreds of nanometers to several micrometers in diameters, as characterized by scanning electron microscopy (SEM) image presented in Figure 22a. Then, a long ZnO micro/nanowire was chosen and dispersed onto a PET/PS substrate; both ends of the ZnO micro/nanowire were fixed by silver paste, serving as electrodes. After that a layer of epoxy was used to fully cover the two silver electrodes, preventing them from exposing in the air during the following test. An as-fabricated ZnO micro/nanowire humidity sensor was sealed in a humidity chamber with one end tightly fixed on the holder as schematically shown in Figure 22b. Piezotronic effect was introduced by bending the other end of

the device through moving a positioner, which was attached to a 3D mechanical stage with movement resolution of 10 μm located outside the chamber, up and down to apply external strains. A typical digital image together with an optical microscopy image focusing on the micro/nanowire and metal electrodes of the device are presented in Figure 22c and d, respectively.

Systematic measurements of humidity sensors were conducted under different RH and strain conditions at room temperature. For a strain free and a −0.20% compressively strain ZnO micro/nanowire humidity sensor, typical I-V characteristics under different RHs are presented in Figure 23a and b, respectively. The derived non-linear and non-symmetrical I-V curves indicate that the barrier heights at two Schottky contacts are distinguishable. The output signals (i.e. current) decreased when increasing the RH in a monotonous manner for both cases, a clear trend can be observed by extracting current value at fixed 2.8 V with drain electrode reversely biased as presented at most right side of Figure 23a and b correspondingly. Under 0.00% strain (Figure 23a), the current decreased from 365.0 nA to 8.72 nA when the RH increased from ∼15.0% to ∼66.0%, while the current decreased from 884 nA to 12.9 nA as shown in Figure 23b, when the humidity sensor was −0.22% compressively strained, which indicates that the piezotronic effect could largely enhance the resolution of the humidity sensor. For a better understanding of the behavior of this humidity sensor, an equivalent circuit model (inset of Figure 23c) is built to fit its I-V characteristics as

plotted in Figure 23c (red line), together with the experimental data in blue dots. Furthermore, the changes of SBH at both ends, Φ_d and Φ_s, as well as the resistance of a strain free ZnO micro/nanowire humidity sensor are also calculated under different RHs as presented in Figure 23d and e. Apparently,

the SBHs changed randomly with the RHs, while the resistance increased with the increasing of RHs.

Figure 24a and c shows the typical I-V characteristics together with the extracted current changes under a fixed 2.8 V bias voltage (drain electrode reversely biased) for two typical
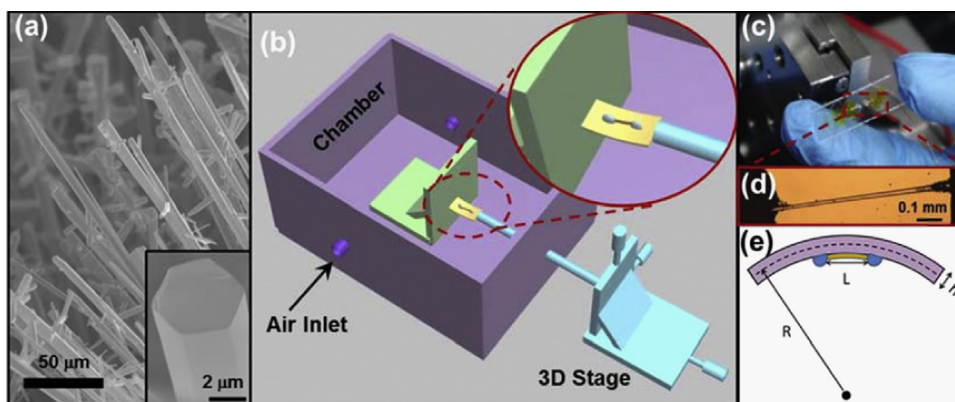
Figure 22 (a) Scanning electron microscopy (SEM) image of the as-grown ZnO NWs. Inset: Enlarged SEM image of an individual ZnO NW, showing a perfect hexagonal cross-section. (b) Schematic of the measurement setups. (c) The optical image of an as-fabricated humidity sensor; (d) The optical microscopy image of the as-fabricated device. (e) Schematic shows the calculation of the compressive strain applied to the device Reproduced with permission from Springer [72].
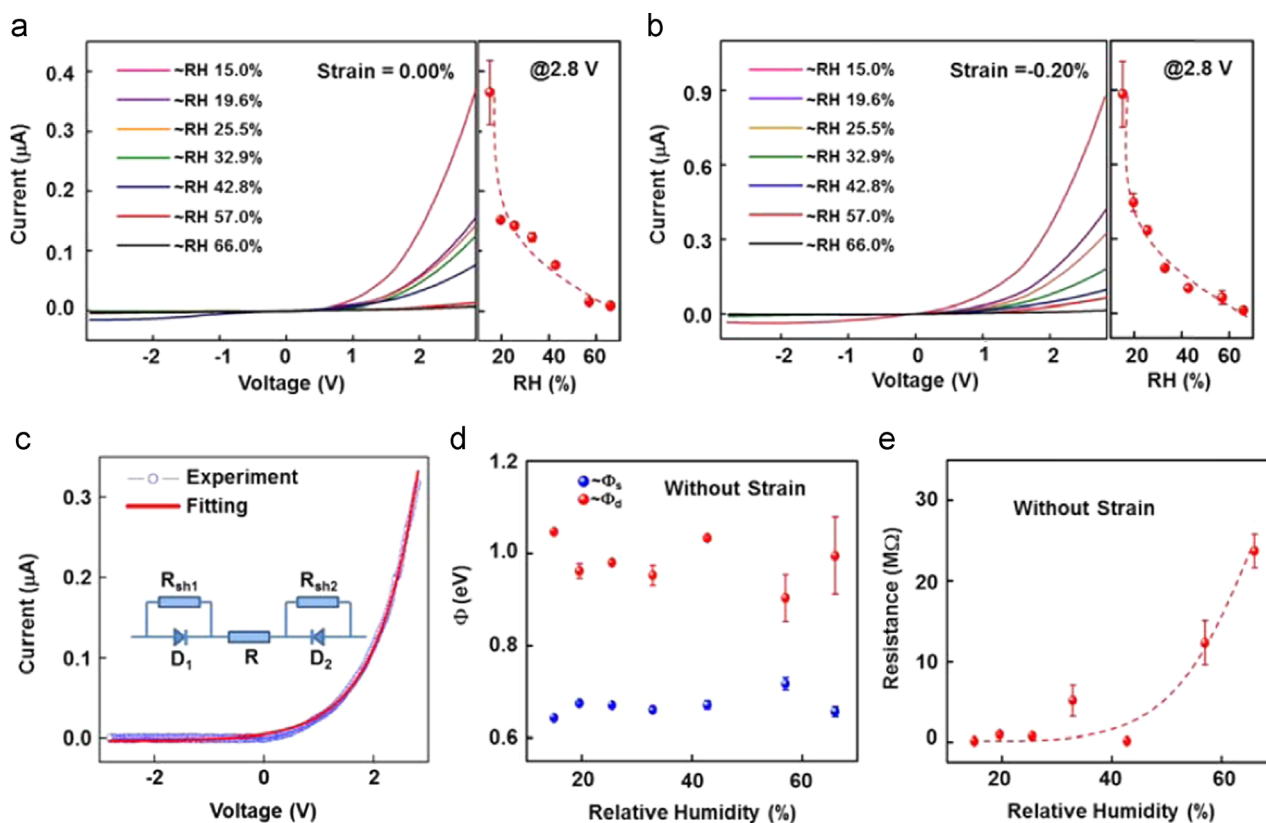
Figure 23 (a, b) I–V curves of the humidity sensor at different RHs, the compressive strain was 0.00% (a) and 0.20% (b) respectively. (c) Equivalent circuit model and quantitative fitting result of an individual ZnO NW-based humidity sensor. (d) The fitting results of the two Schottky barrier height changes with RHs from 15% to 66% without strain. (e) The fitting results of the resistance of the device with RHs from 15% to 66% without strain Reproduced with permission from Springer [72].

humidity RH 25.5% and 32.9%, respectively. It can be seen the output signal increases monotonously with increasing the externally applied compressive strains at a fixed RH when drain electrode was reversely biased. Theoretical simulations were also conducted to derive the changes of SBH at both ends (Figure 24b and d), showing that Φ_d decreased with increasing the compressive strains in both RH cases.

A 3-dimensional (3D) scatter plot is presented in Figure 25a to show the humidity sensor's performances at a fixed bias of 2.8 V under different humidity and strain conditions. The overall trend of output signals changes can be concluded straightforwardly by correlating it with RH and compressive strains. The current monotonously increases with the increment of compressive strain, while decreases with the increment of RH. Two 2D graphs are extracted from Figure 25a to display the outputs response to different compressive strains and RHs under certain circumstances as shown in Figure 25b and c, respectively. These results confirm that piezotronic effect can enhance the general performances of humidity sensors at different RH by rising up the signal levels, and improve the sensing resolution by significantly enlarging the current differences between two RHs under certain strain condition. Moreover, the slope of curves became deeper and deeper when the applied strain increased, which means the sensitivity of humidity sensors was improved by the piezotronic effect as well.

To optimize the performances of the ZnO micro/nanowire humidity sensor, the relative changes of output current with respect to changing compressive strains and RHs are plotted as another two 3D scatter graphs in Figure 25d and f, from which two 2D graphs are extracted as shown in Figure 25e and g. By looking into the relative current response to various RHs under

each certain strain condition, it is obvious to conclude that the larger the compressive strain, the larger the relative changes can be obtained from output signals. Therefore, a −0.22% compressive strain in our case can optimize the performances of ZnO micro/nanowire humidity sensor by achieving a largest responsivity of 1240%.

In this work, by introducing the piezotronic effect, the signal level, sensitivity and sensing resolution of the humidity sensor were largely enhanced by applying an external strain. Since a higher Schottky barrier largely reduces the signal level while a lower Schottky barrier decreases the sensor sensitivity due to increased Ohmic transport, an optimum −0.22% compressive strain was determined to enhance the performances of the humidity sensor with the largest responsivity of 1240%.

Piezotronic effect enhanced temperature sensors [47]

A transfer technique was introduced to fabricate our device, as schematically shown in Figure 26a. Negative photoresist (SUN-9i) as a sacrificial layer was spin-coated onto the PET substrate before the subsequent synthesis of ZnO NW film using the wet chemical deposition method. The bimetallic strip substrate was then attached to the as-synthesized ZnO NW film with epoxy. Next, the sample was dried at room temperature for 12 h to improve epoxy's adhesion to the substrate. Lastly, the sacrificial layer was dissolved by acetone, and the ZnO NW film was successfully transferred from the PET substrate to the bimetallic strip substrate. The photograph of the fabricated device is presented in Figure 26b. This transfer technique successfully
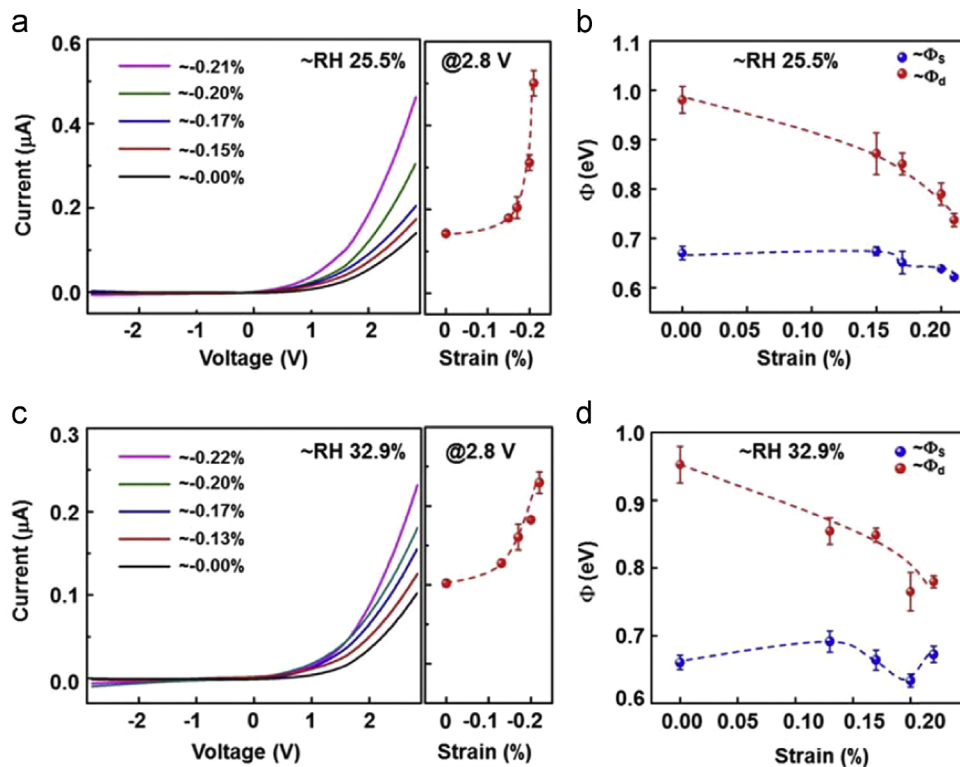

Figure 24 *I–V* curves of the humidity sensor at different compressive strains, the RH was 25.5% (a) and 32.9% (c), respectively. (b, d) The fitting results of the two Schottky barrier height changes with compressive strains from 0% to 0.22%, the RH was 25.5% and 32.9% respectively Reproduced with permission from Springer [72].

introduces a good heat conductor (bimetallic strip) as the substrate and meanwhile overcomes the geometric deformation of ZnO NW film synthesized directly on the bimetallic strip for device fabrication. The cross-sectional and surface morphologies of the ZnO NW film before transfer are presented by scanning electron microscopy (SEM) images in Figure 26c and d. The nanowires are orderly grown and densely ranged as a textured film with the c-axis of the NWs pointing upward [63].

The response of the ZnO NW film based sensor to different temperatures, measured at a fixed bias of 6 V, is presented in Figure 27a. The response signal of the sensor decreased

significantly from a few micro-amperes to dozens of nano-amperes when heating from 10 to 110 °C. This obvious trend is mainly controlled by the piezoelectric polarization charges at the contact interface and thermal disturbance of the sensor. This result indicates that the ZnO NW film based device has a good response to temperature. The relative current change of this sensor was calculated as shown in Figure 27a (blue roundness), which presents a trend of parabola, and the relative current change is as high as 50% from 30 to 70 °C. The ZnO NW film based sensor for the temperature change
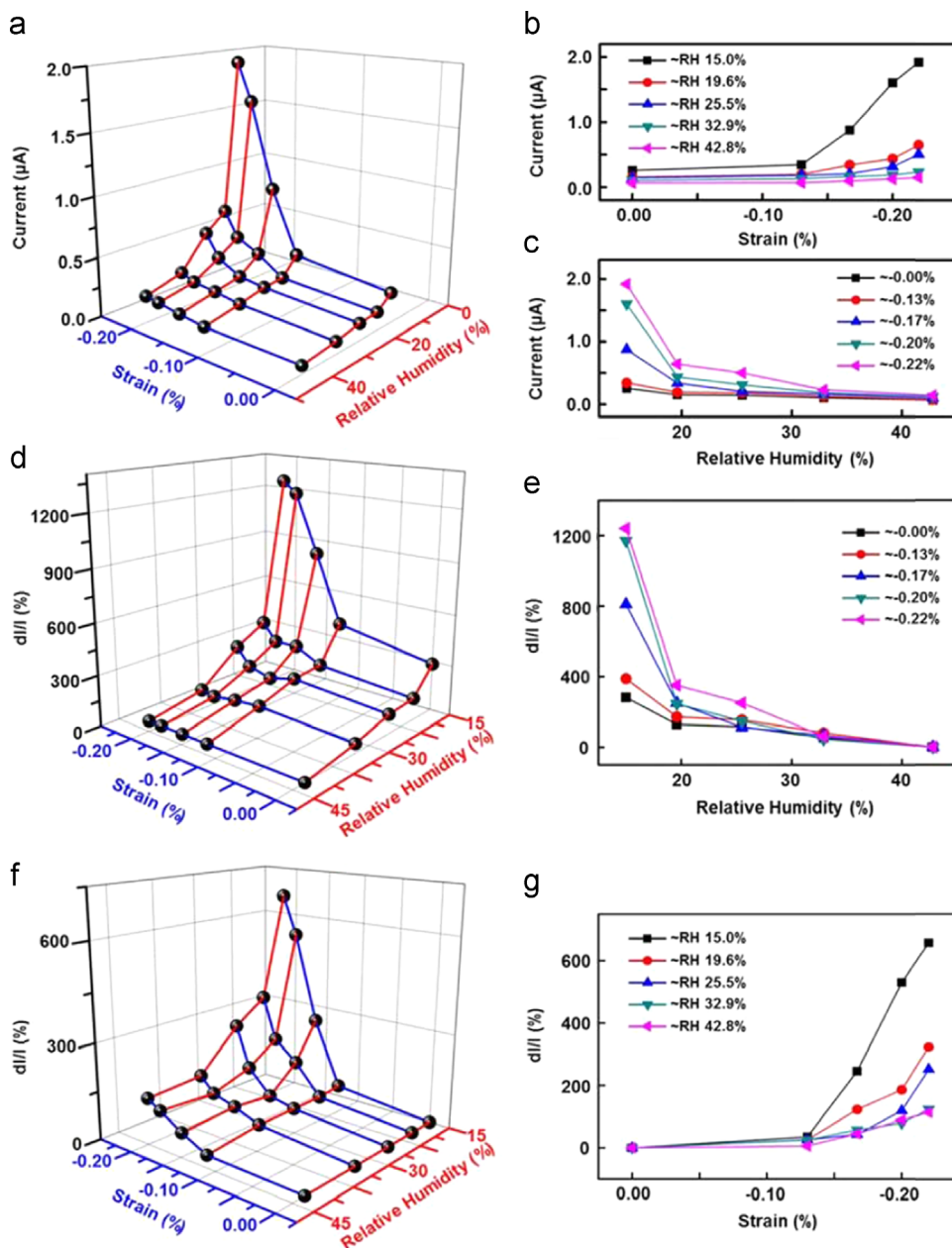
Figure 25 (a) 3D graph depicting the current response of the ZnO NW humidity sensor to strain and relative humidity at a bias voltage of 2.8 V. (b) Absolute current response to different compressive strains, with relative humidity ranging from 15.0% to 42.8%. (c) Absolute current response to different relative humidity, with compressive strains ranging from −0.00% to −0.22%. (d) 3D graph and its corresponding 2D projection (e) indicate the relative changes of current with respect to the value at 42.8% RH, under different compressive strains ranging from −0.00% to −0.22%. (f) 3D graph and its corresponding 2D projection (g) indicate the relative changes of current with respect to the value at 0.0% strain, under different RHs ranging from 15.0% to 42.8% Reproduced with permission from Springer [72].

showed good repeatability with a fixed bias voltage at the source electrode, as illustrated in Figure 27b.

Systematic measurements of the temperature sensor were performed in a temperature test chamber under different temperatures at a fixed relative humidity about 12%. Figure 27c shows *I-V* characteristic at different temperatures. The device presents a typical nonlinear symmetrical *I-V* curve, which indicates that the two Schottky barriers at the two contacts have almost the same heights under the fixed bias voltage. To further demonstrate the ZnO NW film based temperature sensor's performance, the sensitivity under different source bias voltages and different temperatures was plotted in a 3D graph, as shown in Figure 27e. Under a certain temperature, the sensitivity gradually increased with the increase of bias voltages, among which the maximum and the minimum incredibly reached 3.05%/°C and 0.98%/°C, which are about 10 times and 3 times, respectively, higher than responses of the temperature sensors on the market, such as PT100 based thermometers. At a fixed bias voltage, the sensitivity first increased to the maximum value with the rise of temperature and then gradually decreased when temperature exceeded 30 °C, which is determined by the properties of the bimetallic strip. The deformations of our practical device under different temperatures are shown in Figure 27f.

In order to confirm the dominant factor that determines the current change of temperature sensors, two groups of devices were fabricated for comparison. First, an Ohmic-contacted device was characterized under different bias voltages and different temperatures as shown in Figure 28a. The variation of the current signal under a fixed bias voltage is illustrated in Figure 28b, fitting a parabolic function with the temperature, which indicates that with the increase of the temperature, the mobility of the carriers (electron) increases at low temperatures and then decreases at high temperatures in accordance with the previous report. Next, as a control experiment, ZnO NW films were transferred to silicon and aluminum oxide to fabricate Schottky-contacted devices. *I-V* characteristics of a silicon substrate device are presented in Figure 28c. These results can be explained as follows: at low temperatures, with the increase of temperature, the Fermi level and band gap of the metal and semiconductor remain little changed while the mobility of the carrier (electron) increases rapidly, resulting in the increased current. At high temperatures, with the increase of temperature, the mobility of the carrier decreases gradually while the lowered Fermi level and the shrinkage band gap lead to the rise of the Schottky barriers, resulting in the decreased current. Detailed current changes compared with the bimetallic strip substrate based temperature sensor are illustrated in Figure 28d. The bimetallic strip based device exhibits a more distinct current change than the silicon based one, indicating an obvious enhancement of the performances by piezotronic effect.

From this work, the primary role of piezotronic effect over geometrical and piezoresistive effect in the as fabricated devices has been confirmed, and piezotronic effect on charge carrier transportation under different strains is subsequently studied. In addition, we also presented that the temperature sensing capability of as-fabricated NW film based piezotronic devices can be tuned by piezopotential, which exhibits dramatically enhanced sensitivity.
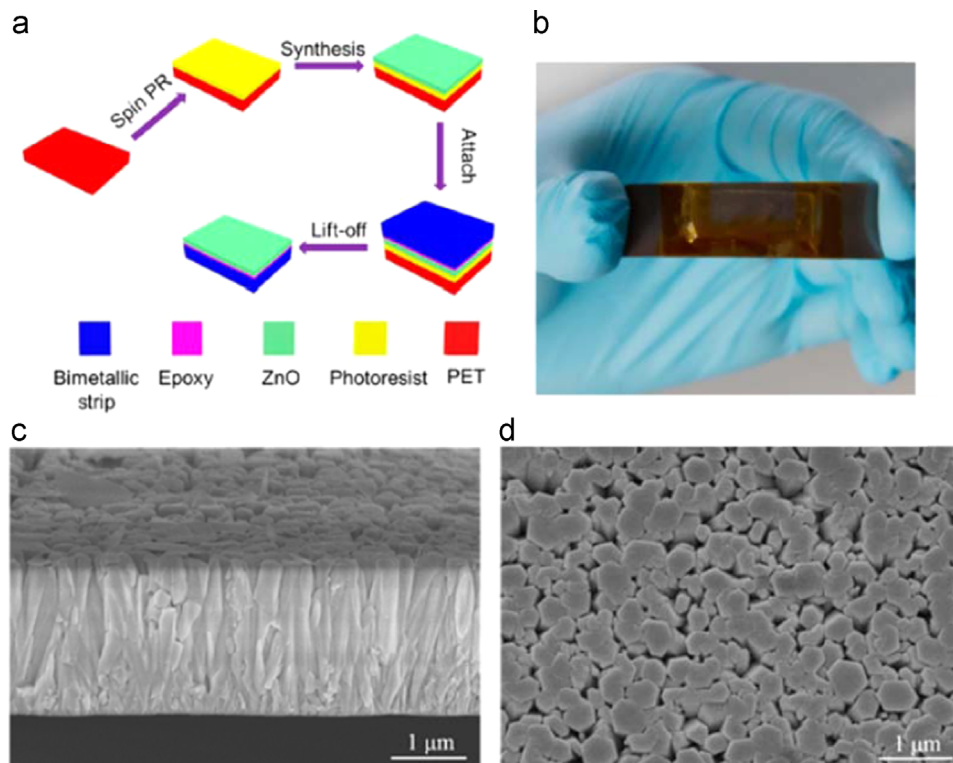
Figure 26 (a) Schematically illustration of transfer process of ZnO NW film from PET to the bimetallic strip. (b) Photograph of an as-fabricated device. (c, d) SEM images of as-synthesized ZnO nanowire film Reproduced with permission from American Chemical Society [73].
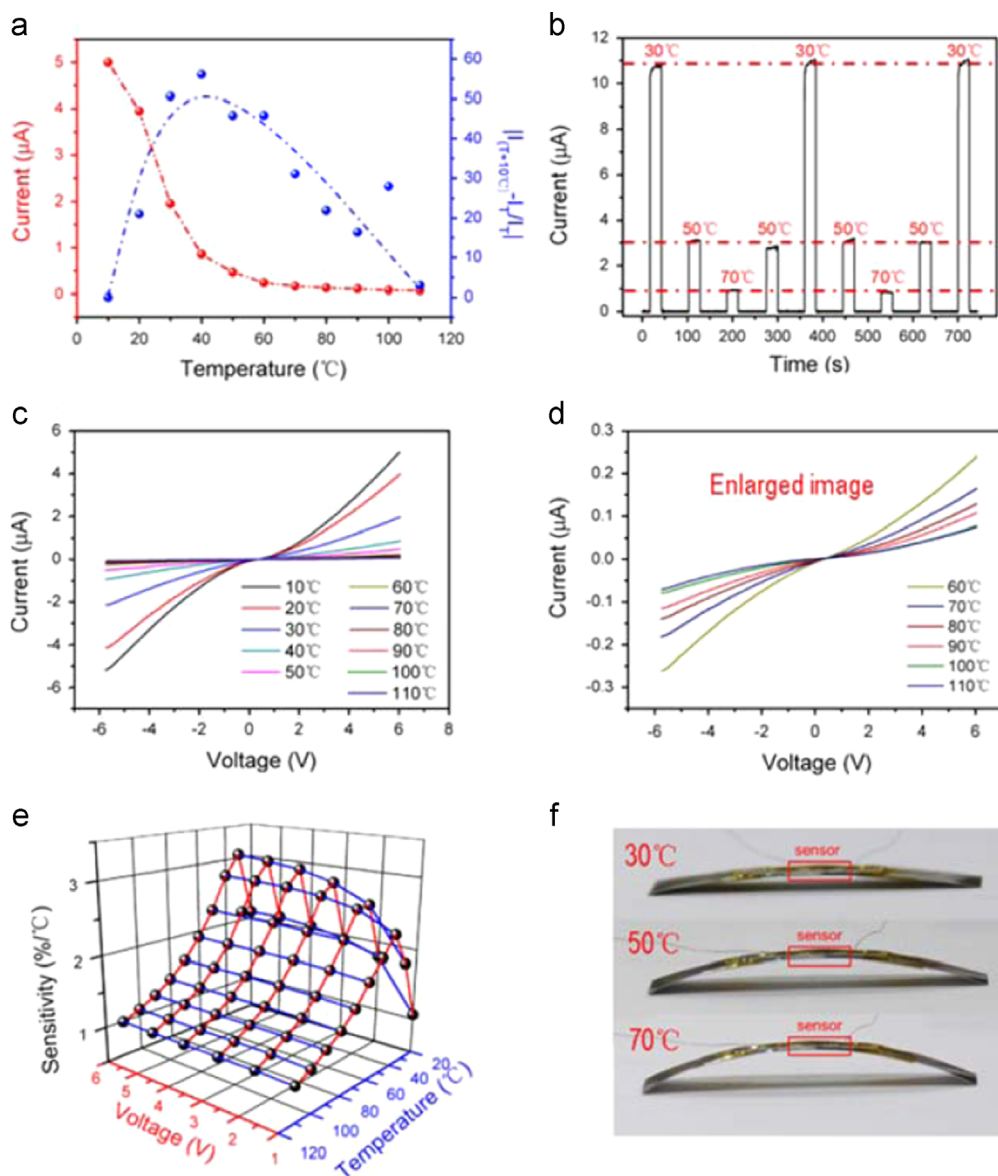
Figure 27 (a) Response and relative current change of the sensor to the temperature, varying from 10 to 110 °C. (b) Repeatability of the temperature sensor at fixed bias voltage. (c) $I-V$ curves of the sensor at different temperatures. (d) Enlarged image of c from 60 to 110 °C. (e) The normalized average sensitivity of the sensor at different bias voltages and different temperatures. (f) Deformation of the practical sensor at different temperatures. The bimetallic strip was 5.5 cm in length and 2 cm in width, while the ZnO NW film was about 1 cm in length and 0.5 cm in width Reproduced with permission from American Chemical Society [73].

Summary and perspective

Today's one dimensional NW sensors mainly utilizes the surface effect with Ohmic contacts and the current change is mainly due to the change of NW resistance, which is essentially an volume effect of the NW. Utilizing Schottky contact, the sensitivity of NW sensor is enhanced by as much as 4 orders of magnitudes [12] compared with the Ohmic contact devices. By introducing the piezotronic effect to tune the Schottky barrier height through piezo-polarization charges, the already high sensitivity is further improved by more than 300% [64].

Prototype piezotronic-enhanced Schottky sensors have already been demonstrated in various applications. We anticipated this NW device structure can be further optimized to reach a higher sensitivity in future researches. The piezoelectric NW material system can be further broadened to demonstrate this kind of sensors in wider applications. Besides single NW devices, these integrated NW sensor array system can have further applications in chemical species and strain mapping. And thin film piezotronic-enhanced Schottky sensors can also be demonstrated. These kind of piezotronic-enhanced Schottky sensors are likely to have important applications in ultra-sensitive sensor application, human-machine interfacing, MEMS, nanorobotics, and flexible electronics.

Acknowledgments
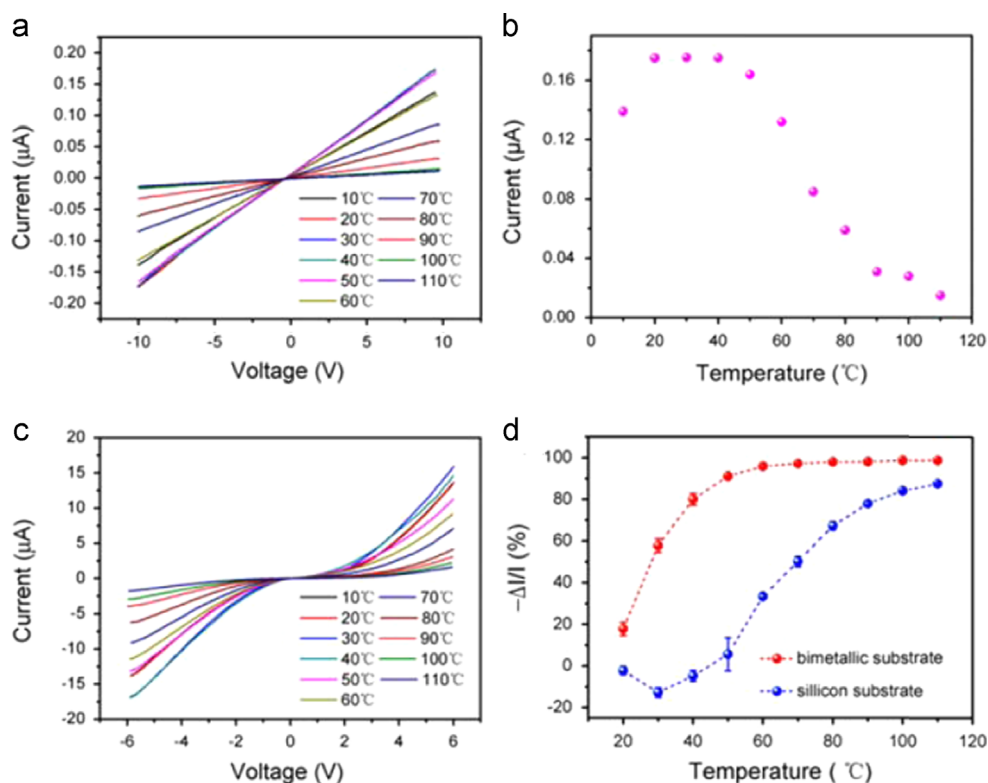
Figure 28 (a) $I-V$ curves of the device with Ohmic contact at different temperatures. (b) The current signals of the device with Ohmic contact under a fixed bias voltage at different temperatures. (c) $I-V$ curves of the device with Schottky contact and silicon substrate at different temperatures. (d) Normalized current change at different temperatures. The blue curve represents the device with a silicon substrate; the red represents the device with a bimetallic strip substrate Reproduced with permission from American Chemical Society [73].

References

[1] Y. Cui, C.M. Lieber, Science 291 (5505) (2001) 851-853.
[2] X. Duan, Y. Huang, Y. Cui, J. Wang, C.M. Lieber, Nature 409 (6816) (2001) 66-69.
[3] M.S. Arnold, P. Avouris, Z.W. Pan, Z.L. Wang, J. Phys. Chem. B 107 (3) (2003) 659-663.
[4] Q. Kuang, C. Lao, Z.L. Wang, Z. Xie, L. Zheng, J. Am. Chem. Soc. 129 (19) (2007) 6070-6071.
[5] J. Yu, M. Shafiei, C.M. Oh, T.B. Jung, K. Kalantar-Zadeh J.H. Kang, W. Wlodarski, Sens. Lett. 9 (1) (2011) 55-58.
[6] R.K. Gupta, F. Yakuphanoglu, Sol. Energy 86 (5) (2012) 1539-1545.
[7] H.D. Fard, S. Khatami, N. Izadi, J. Koohsorkhi, A. Rashidi, Sens. Mater. 25 (5) (2013) 297-308.
[8] F. Zorgiebel, S. Pregl, L. Romhildt, J. Opitz, W. Weber, T. Mikolajick, L. Baraban, G. Cuniberti, Nano Res. 7 (2) (2014) 263-271.
[9] A. Singh, M.A. Uddin, T. Sudarshan, G. Koley, Small 10 (8) (2014) 1555-1565.
[10] K. Momeni, H. Attariani, Phys. Chem. Chem. Phys. 16 (10) (2014) 4522-4527.
[11] N.J. Ku, J.H. Huang, C.H. Wang, H.C. Fang, C.P. Liu, Nano Lett. 12 (2) (2012) 562-568.
[12] Z.L. Wang, INEC: 2010 3rd International Nanoelectronics Conference, vols. 1 and 2, 2010, pp. 63-64.
[13] R. Yu, C. Pan, J. Chen, G. Zhu, Z.L. Wang, Adv. Funct. Mater. 23 (47) (2013) 5868-5874.
[14] R. Yu, C. Pan, Z.L. Wang, Energy Environ. Sci. 6 (2) (2013) 494-499.
[15] C. Pan, R. Yu, S. Niu, G. Zhu, Z.L. Wang, ACS Nano 7 (2) (2013) 1803-1810.
[16] Z.L. Wang, Adv. Mater. 19 (6) (2007) 889-892.
[17] Z.L. Wang, Adv. Mater. 24 (34) (2012) 4632-4646.
[18] Y. Cui, Q.Q. Wei, H.K. Park, C.M. Lieber, Science 293 (5533) (2001) 1289-1292.
[19] C.M. Lieber, MRS Bull. 28 (7) (2003) 486-491.
[20] G.F. Zheng, F. Patolsky, Y. Cui, W.U. Wang, C.M. Lieber, Nat. Biotechnol. 23 (10) (2005) 1294-1301.
[21] F. Patolsky, C.M. Lieber, Mater. Today 8 (4) (2005) 20-28.
[22] M. Curreli, C. Li, Y.H. Sun, B. Lei, M.A. Gundersen, M.E. Thompson, C.W. Zhou, J. Am. Chem. Soc. 127 (19) (2005) 6922-6923.
[23] J.H. He, Y.Y. Zhang, J. Liu, D. Moore, G. Bao, Z.L. Wang J. Phys. Chem. C 111 (33) (2007) 12152-12156.
[24] I. Heller, A.M. Janssens, J. Mannik, E.D. Minot, S.G. Lemay, C. Dekker, Nano Lett. 8 (2) (2008) 591-595.
[25] E.L. Gui, L.J. Li, K.K. Zhang, Y.P. Xu, X.C. Dong, X.N. Ho P.S. Lee, J. Kasim, Z.X. Shen, J.A. Rogers, S.G. Mhaisalkar J. Am. Chem. Soc. 129 (46) (2007) 14427-14432.
[26] R.J. Chen, H.C. Choi, S. Bangsaruntip, E. Yenilmez, X.W. Tang, Q. Wang, Y.L. Chang, H.J. Dai, J. Am. Chem. Soc. 126 (5) (2004) 1563-1568.

[27] H.R. Byon, H.C. Choi, J. Am. Chem. Soc. 128 (7) (2006) 2188-2189.

[28] X.W. Tang, S. Bansaruntip, N. Nakayama, E. Yenilmez, Y.L. Chang, Q. Wang, Nano Lett. 6 (8) (2006) 1632-1636.

[29] X.F. Duan, Y. Huang, Y. Cui, J.F. Wang, C.M. Lieber, Nature 409 (6816) (2001) 66-69.

[30] M.S. Arnold, P. Avouris, Z.W. Pan, Z.L. Wang, J. Phys. Chem. B 107 (3) (2003) 659-663.

[31] A.B. Artyukhin, M. Stadermann, R.W. Friddle, P. Stroeve, O. Bakajin, A. Noy, Nano Lett. 6 (9) (2006) 2080-2085.

[32] Q. Kuang, C.S. Lao, Z.L. Wang, Z.X. Xie, L.S. Zheng, J. Am. Chem. Soc. 129 (19) (2007) 6070.

[33] J. Zhou, Y.D. Gu, P. Fei, W.J. Mai, Y.F. Gao, R.S. Yang, G. Bao, Z.L. Wang, Nano Lett. 8 (9) (2008) 3035-3040.

[34] J. Zhou, Y.D. Gu, Y.F. Hu, W.J. Mai, P.H. Yeh, G. Bao, A.K. Sood, D.L. Polla, Z.L. Wang, Appl. Phys. Lett. 94 (19) (2009) 191103.

[35] Z.W. Pan, Z.R. Dai, Z.L. Wang, Science 291 (5510) (2001) 1947-1949.

[36] Q.H. Li, T. Gao, Y.G. Wang, T.H. Wang, Appl. Phys. Lett. 86 (12) (2005) 123117.

[37] Y.Z. Jin, J.P. Wang, B.Q. Sun, J.C. Blakesley, N.C. Greenham, Nano Lett. 8 (6) (2008) 1649-1653.

[38] Z.Y. Fan, J.G. Lu, Appl. Phys. Lett. 86 (3) (2005).

[39] R.W.J. Scott, S.M. Yang, G. Chabanis, N. Coombs, D.E. Williams, G.A. Ozin, Adv. Mater. 13 (19) (2001) 1468 -+.

[40] Q. Wan, Q.H. Li, Y.J. Chen, T.H. Wang, X.L. He, J.P. Li, C. L. Lin, Appl. Phys. Lett. 84 (18) (2004) 3654-3656.

[41] B. Wang, L.F. Zhu, Y.H. Yang, N.S. Xu, G.W. Yang, J. Phys. Chem. C 112 (17) (2008) 6643-6647.

[42] C.F. Pan, R.M. Yu, S.M. Niu, G. Zhu, Z.L. Wang, ACS Nano 7 (2) (2013) 1803-1810.

[43] R.M. Yu, C.F. Pan, J. Chen, G. Zhu, Z.L. Wang, Adv. Funct. Mater. 23 (47) (2013) 5868-5874.

[44] R.M. Yu, C.F. Pan, Z.L. Wang, Energy Environ. Sci. 6 (2) (2013) 494-499.

[45] S.M. Niu, Y.F. Hu, X.N. Wen, Y.S. Zhou, F. Zhang, L. Lin S.H. Wang, Z.L. Wang, Adv. Mater. 25 (27) (2013) 3701-3706.

[46] G.F. Hu, R.R. Zhou, R.M. Yu, L. Dong, C.F. Pan, Z.L. Wang, Nano Res. 7 (7) (2014) 1083-1091.

[47] F. Xue, L.M. Zhang, W. Tang, C. Zhang, W.M. Du, Z.L. Wang, ACS Appl. Mater. Interfaces 6 (8) (2014) 5955-5961.

[48] S. Xu, Y. Qin, C. Xu, Y.G. Wei, R.S. Yang, Z.L. Wang, Nat. Nanotechnol. 5 (5) (2010) 366-373.

[49] R.S. Yang, Y. Qin, L.M. Dai, Z.L. Wang, Nat. Nanotechnol. 4 (1) (2009) 34-39.

[50] R.M. Yu, L. Dong, C.F. Pan, S.M. Niu, H.F. Liu, W. Liu, S. Chua, D.Z. Chi, Z.L. Wang, Adv. Mater. 24 (26) (2012) 3532-3537.

[51] Y. Liu, Z.Y. Zhang, Y.F. Hu, C.H. Jin, L.M. Peng, J. Nanosci. Nanotechnol. 8 (1) (2008) 252-258.

[52] X.D. Han, K. Zheng, Y.F. Zhang, X.N. Zhang, Z. Zhang, Z.L. Wang, Adv. Mater. 19 (16) (2007) 2112 +.

[53] Z.Y. Zhang, C.H. Jin, X.L. Liang, Q. Chen, L.M. Peng, Appl. Phys. Lett. 88 (7) (2006) 073102.

[54] M. Eichenfield, J. Chan, R.M. Camacho, K.J. Vahala, O. Painter, Nature 462 (7269) (2009) 78-82.

[55] Y.M. Sung, K. Noh, W.C. Kwak, T.G. Kim, Sens. Actuators B—Chem. 161 (1) (2012) 453-459.

[56] S. Mao, G.H. Lu, K.H. Yu, Z. Bo, J.H. Chen, Adv. Mater. 22 (32) (2010) 3521 +.

[57] J.X. Chen, L.W. Ding, X.H. Zhang, L. Chu, N.S. Liu, Y.H. Gao, Opt. Express 22 (2014) 3661-3668.

[58] C.F. Pan, Z.T. Li, W.X. Guo, J. Zhu, Z.L. Wang, Angew. Chem. Int. Ed. 50 (47) (2011) 11192-11196.

[59] Y.F. Hu, Y. Liu, W.L. Li, M. Gao, X.L. Liang, Q. Li, L.M. Peng, Adv. Funct. Mater. 19 (15) (2009) 2380-2387.

[60] C.Y. Lu, S.P. Chang, S.J. Chang, T.J. Hsueh, C.L. Hsu, Y.Z. Chiou, C. Chen, IEEE Sens. J. 9 (4) (2009) 485-489.

[61] L.M. Wu, F.F. Song, X.X. Fang, Z.X. Guo, S. Liang, Nanotechnology 21 (47) (2010) 475502.

[62] K.W. Liu, M. Sakurai, M. Aono, Sens. Actuators B 157 (1) (2011) 98-102.

[63] L. Vayssieres, Adv. Mater. 15 (5) (2003) 464-466.

[64] Z.L. Wang, Abstr. Pap. Am. Chem. S 238 (2009).

[65] Z.L. Wang, Microsc. Microanal. 15 (2009) 1152-1153.

[66] J. Volk, T. Nagata, R. Erdelyi, I. Barsony, A.L. Toth, I.E. Lukacs, Z. Czigany, H. Tomimoto, Y. Shingaya, T. Chikyow, Nanoscale Res. Lett. 4 (7) (2009) 699-704.

[67] Z.L. Wang, Adv. Funct. Mater. 18 (22) (2008) 3553-3567.

[68] Z.L. Wang, Abstr. Pap. Am. Chem. S 235 (2008).

[69] Z.L. Wang, Advances in Heterogeneous Material Mechanics 2008, 2008, p. 69.

[70] Y. Gao, Z.L. Wang, Nano Lett. 7 (8) (2007) 2499-2505.

[71] Z.L. Wang, Mater. Today 10 (5) (2007) 20-28.

[72] Z.L. Wang, Proceedings of 2007 IEEE International Electron Devices Meeting, vols. 1 and 2, 2007, pp. 371-374.

[73] R.M. Yu, W.Z. Wu, Y. Ding, Z.L. Wang, ACS Nano 7 (7) (2013) 6403-6409.

Ruomeng Yu is a Ph.D. candidate working as a graduate research assistant in the School of Materials Science and Engineering at Georgia Institute of Technology, under the supervision of Prof. Zhong Lin Wang. He received his B.S. degree in Applied Physics from Huazhong University of Science and Technology in 2010, and his M.S. degree in Physics from Georgia Institute of Technology in 2012. His research interests include synthesis, fabrication and integration of nanomaterials/electronic devices; nano/micro-scale electronics for energy harvesting/conversion/storage; self-powered sensing systems; mechanical/optical signals-controlled logic circuits; optoelectronics; piezotronics/piezo-photonics/piezo-phototronics.
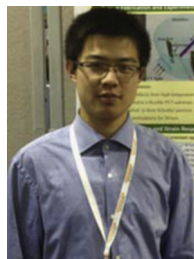
Simiao Niu is a Ph.D. candidate working as a graduate research assistant in School of Materials Science and Engineering at the Georgia Institute of Technology, under the supervision of Prof. Zhong Lin Wang. He earned his B.E. degree in the Institute of Microelectronics at Tsinghua University in 2011 with the highest honors and outstanding undergraduate thesis award. His doctoral research interests include theoretical and experimental studies on: mechanical energy harvesting by triboelectric nanogenerators and high-performance piezotronic and piezo-phototronic sensors based on piezoelectric nanowires.

Dr. Caofeng Pan received his B.S. degree (2005) and his Ph.D. (2010) in Materials Science and Engineering from Tsinghua University, China. He then joined in the group of Professor Zhong Lin Wang at the Georgia Institute of Technology as a postdoctoral fellow. He is currently a professor and a group leader at Beijing Institute of Nanoenergy and Nanosystems, Chinese Academy of Sciences since 2013. His main research interests focus on the fields of piezotronics/piezo-phototronics for fabricating new electronic and optoelectronic devices, nano-power source (such as nanofuel cell, nano biofuel cell and nanogenerator), hybrid nanogenerators, and self-powered nanosystems. Details can be found at http://piezotronics.binncas.cn/index%20en.php.

Dr. Zhong Lin (ZL) Wang is the Hightower Chair in Materials Science and Engineering, Regents' Professor, at Georgia Tech. He is also the chi ef scientist and director of Beijing Institute of Nanoenergy and Nano-systems, Chinese Academy of Sciences. Dr. Wang has the original and innovative contributions to the synthesis, discovery, characterization and understanding of fundamental physical properties of oxide nanobelts and nanowires, as well as applications of nanowires in energy sciences, electronics, optoelectronics and biological science. He is the leader figure in ZnO nanostructure research. His discovery and breakthroughs in developing nanogenerators establish the principle and technological road map for harvesting mechanical energy from environment and biological systems for powering a personal electronics. His research on self-powered nanosystems has inspired the worldwide effort in academia and industry for studying energy for micro-nano-systems, which is now a distinct disciplinary in energy research and future sensor networks. He coined and pioneered the field of piezotronics and piezo-phototronics by introducing piezoelectric potential gated charge transport process in fabricating new electronic and optoelectronic devices. This historical breakthrough by redesign CMOS transistor has important applications in smart MEMS/NEMS, nanorobotics, human-electronics interface and sensors. Wang also invented and pioneered the in-situ technique for measuring the mechanical and electrical properties of a single nanotube/nanowire inside a transmission electron microscope (TEM).